WCAP-16045-NP-A, Addendum 2 June 2019

Revision 0

Updated NEXUS Cross-Section Methodology

WCAP-16045-NP-A, Addendum 2
Revision 0

Updated NEXUS Cross-Section Methodology

Authors:
Baocheng Zhang
Gary Mangham
PWR Core Methods, Technology and Licensing

June 2019

Reviewer: Vefa Kucukboyaci
PWR Core Methods, Technology and Licensing
Bradley Maurer
Product Line Regulatory Support

Approved: Zachary B. McDaniel, Manager
PWR Core Methods, Technology and Licensing

.

*Electronically approved records are authenticated in the electronic document management system.

Westinghouse Electric Company LLC
1000 Westinghouse Drive
Cranberry Township, PA 16066, USA

TABLE OF CONTENTS

LIST OF TABLES

LIST OF FIGURES

1 INTRODUCTION

The NEXUS methodology is a reparameterization of the PARAGON (Reference 4) nuclear data output and a new reconstruction approach within the ANC core simulator code (Reference 1) to simplify the use of this code system for design use. The current version of the NEXUS methodology (Reference 2) has been licensed by the NRC for uranium-fueled pressurized water reactors (PWRs).

The NEXUS methodology provides a linkage between the lattice code PARAGON and ANC. PARAGON is a stand-alone neutron transport code based on collision probability techniques and approved for use as a stand-alone lattice physics code and as a cross-section generation tool for core simulators, such as ANC, for uranium-fueled PWRs. ANC is a core simulator code system which performs calculations based on nuclear data supplied by a code such as PARAGON or PHOENIX-P.

Westinghouse has developed an improved version of the NEXUS cross-section methodology, referred to in this report as Updated NEXUS. This updated methodology will enable NEXUS to:

- Model accident conditions with high local void or core pressure change
- More effectively capture the effect of each individual physics parameter
- Consistently and efficiently provide more accurate cross-sections at any core condition

The improved NEXUS cross-section methodology, i.e., reformulation and rehomogenization methodology, has been developed and qualified. Westinghouse is seeking an approval of the updated NEXUS methodology to be used in the NEXUS/ANC code system, as a direct replacement of all existing uses of the currently licensed NEXUS methodology in References 2 and 3 for both normal operating and accident conditions.

2 METHODOLOGY

2.1 CROSS–SECTION DATA REFORMULATION

2.1.1 Currently Licensed NEXUS Methodology

NEXUS adopts a once-through cross-section representation methodology to generate node-wise two-group assembly nuclear data for Westinghouse nodal code ANC (Reference 1). These assembly average nuclear data, e.g., cross-sections, vary with the local neutron spectrum. The current licensed cross-section methodology (Reference 2) characterizes the local spectrum using three node-average state parameters: (1) spectrum index (SI), the ratio of fast-to-thermal group node-average fluxes, (2) fuel temperature (T_f), and (3) moderator temperature (T_m). This methodology has been successfully applied to pressurized water reactor core design and safety analysis and provides accurate predictions in steady-state operation conditions. However, it is desirable to expand the current NEXUS capability to be able to precisely model an accident condition with high local void or core pressure change (Reference 5). This will enable elimination of overly conservative cross-section calculations.

The SI represents the overall shape of the neutron spectrum and is affected by any physical state parameter (e.g., boron concentration, moderator density, temperatures, actual fuel history). Since the spectrum index is not separable, the current methodology has a significant challenge for the advanced application of NEXUS methodology, especially when the explicit feedback or perturbation is needed from an individual physics parameter. Moreover, the spectrum index is a calculated state parameter rather than a physical one that can be controlled by the user. Consequently, the nodal code is required to perform extra feedback iterations to calculate an updated spectrum index in order to reconstruct nodal nuclear data so as to match the actual local conditions, which reduces the code calculation efficiency.

2.1.2 Updated NEXUS Cross-Section Methodology

[

]^{a,c} Extensive studies (Reference 5) have shown that the local spectrum, even at highly voided conditions, can be represented and parameterized using the following four physical local state parameters:

1) [

]^{a,c}

In order to capture the individual feedback effects of these physical state parameters and avoid double-counting these feedback effects in the simulator cross-section representations, the so-called feedback-free macroscopic cross-sections are adopted using a process similar to currently licensed NEXUS. These feedback-free cross-sections along with microscopic cross-sections of the actinides, fission-products, burnable absorbers, and other explicitly modeled isotopes, are a function of the local neutron spectrum. The local spectrum is determined by the above four local state parameters.

The nodal macroscopic cross-section is deconstructed into a feedback-free cross-section and a number of additive feedback correction terms. The feedback-free cross-section and the fundamental components of the feedback correction terms are all given as the product of a reference cross-section and a spectrum correction factor, which is represented in terms of the above four state parameters and fuel exposure.

When modeled in the nodal code, the feedback-included macroscopic cross-sections for each node are reconstructed by correcting the reference feedback-free macroscopic cross-section using the actual conditions of the node.

Additional feedback corrections are added to this cross-section to account for the composition difference from the feedback-free contents. These feedbacks include **[** **]**[a,c] using spectral and history corrected microscopic cross-sections and the corresponding isotopic number densities which are tracked individually for each node in the nodal code. All burnable absorbers are tracked explicitly, and corrections are made to the macroscopic cross-sections for their presence. Macroscopic cross-sections are also corrected for spacer grids and inserted control rods. Finally, the macroscopic cross-section is corrected for the spectral history of the node. All feedback-included macroscopic cross-sections (absorption, fission, etc.) are corrected in this way. The fast and thermal diffusion coefficients are also reconstructed in the same manner.

The fundamental feedback corrections are the microscopic cross-sections representative of the feedback material (i.e., **[** **]**[a,c]). Analogous to the macroscopic cross-sections, these microscopic cross-sections are corrected from the reference microscopic cross-sections. The corrections to the microscopic cross-sections include a spectral correction based on the **[** **]** Corrections are also made to the microscopic cross-sections based on the presence of a spacer grid and/or absorber inserts (e.g., control rod), and/or removal of discrete burnable absorber rods.

Due to thermal expansion, there is a geometry difference between hot and cold conditions; therefore, **[** **]**[a,c] is introduced to the macroscopic cross-sections based on the temperature difference between the reference and actual conditions. With all of the above feedback corrections, the reconstructed macroscopic cross-sections will represent the fuel node at the local conditions at hot dimensions.

As in the currently licensed NEXUS, the corrections for these models are calculated from data generated by the lattice code through the execution of a standardized set of lattice code calculations called the calculational matrix. This matrix includes:

1) [

] a,c

In addition, for the Updated NEXUS methodology, the calculational matrix also includes:

8) [

] a,c

All cases are performed over the exposure range of the reference depletion.

Cross-section data are prepared for the core simulator by performing multivariable least squares fits at each exposure point from the lattice code data. The fit for each correction term is calculated using the data from the appropriate branch cases which calculate the effect of that correction. All corrections are made using the reference depletion data as the base.

Depletion history effects are captured in the nodal simulator by explicitly tracking the number densities of actinides and fission products, as well as all burnable absorber nuclides on a node basis. The macroscopic cross-sections for every node in the nodal simulator are adjusted for these feedback effects by using the differences in the node-wise tracked nuclides from their corresponding reference values at the same fuel burnup and the microscopic cross-sections adjusted to the node conditions. A full set of microscopic data including the microscopic cross-section corrections described above is provided for each fission product and actinide isotope tracked by the simulator.

The reconstruction of the cross-sections in NEXUS/ANC is performed using exactly the same fitting formulations that were used in generating the fitting data from the calculational matrix lattice code data. A significant fraction of the qualification effort involves confirming that the lattice code data is accurately reconstructed by ANC. The results of k-infinity comparisons of ANC single assembly calculations against PARAGON calculations performed at identical conditions are presented for several assembly types and configurations in Section 3 of this report. These calculations demonstrate the accuracy of the NEXUS methodology in reproducing the PARAGON results over a wide range of feedback conditions.

2.2 CROSS-SECTION DATA RE-HOMOGENIZATION

As a standard process, reflective boundary conditions are normally used in lattice calculations. With all the feedback data generated from the standard lattice calculations, the reconstructed cross-sections of NEXUS/ANC represent the fuel assembly at a reflective boundary. When there is a strong interaction between the fuel assembly and its surroundings, the reconstructed nodal average cross-sections in NEXUS/ANC do not account for the environmental effect since the interaction impacts both neutron spectrum and flux distribution in the node. The accuracy of the reconstructed cross-sections has been enhanced by the adoption of a re-homogenization methodology.

Theoretically, the nodal homogenous cross-section (Σ_x) is the flux-volume averaged cross-section from the actual fine mesh cross-sections (Σ_x^i) and fluxes (ϕ^i) as:

$$\Sigma_x = \frac{\sum_i \Sigma_x^i \phi^i V^i}{\sum_i \phi^i V^i}$$

[

] [a,c]

A 3x3 mini-core model is simulated in Section 3.2 to demonstrate the effect and improved accuracy of the cross-section re-homogenization methodology by comparing k-infinity values and assembly power distributions between ANC and PARAGON calculations.

3 QUALIFICATION

3.1 SINGLE ASSEMBLY MODEL CALCULATIONS

The fundamental methodology of updated NEXUS was validated and qualified through single-assembly calculations and directly comparing the results against references that were generated by the PARAGON lattice code. Single-assembly 2D models, assuming reflective boundary conditions, were created using both ANC (using the new NEXUS methodology) and PARAGON. The following fuel lattices were modeled and analyzed in this report:

Lattice 1: Westinghouse-type 17x17 OFA assembly
Enrichment: 5.0 w/o ^{235}U
Burnable absorber: 156 1.5x IFBA, 24 WABA
Reason for inclusion: 17x17 OFA fuel assembly, high enrichment, very high burnable poison loading

Lattice 2: Westinghouse-type 14x14 assembly
Enrichment: 4.0 w/o ^{235}U
Burnable absorber: 64 IFBA
Reasons for inclusion: Even lattice Westinghouse assembly with moderate enrichment and burnable absorber loading

Lattice 3: Westinghouse-type 15x15 assembly
Enrichment: 4.5 w/o
Burnable absorber: 116 IFBA
Reasons for inclusion: 15x15, high power density, high enrichment, high BA loading

Lattice 4: Combustion Engineering-type 16x16 assembly
Enrichment: 4.2 w/o (average)
Burnable absorber: 16 6w/o Gd_2O_3 rods
Reasons for inclusion: CE assembly, heavy Gd_2O_3 burnable absorber loading

Lattice 5: Westinghouse-type 17x17 standard-size fuel rod assembly
Enrichment: 4.95 w/o ^{235}U
Burnable absorber: 48 IFBA
Reasons for inclusion: 17x17 standard rod with high enrichment and light/moderate IFBA loading

Lattice 6: Westinghouse-type 17x17 OFA assembly
Enrichment: 2.6 w/o ^{235}U
Burnable absorber: None
Reasons for inclusion: low enrichment (often used as axial blanket enrichment)

3.1.1 Full Power and Off-Power Depletions

The fuel lattices were depleted at power conditions equivalent to typical reactor operation with various reactor coolant system (RCS) soluble boron levels. The capability of NEXUS to correct the cross-sections for spectral differences permits accurate calculations, at powers other than full power. This is especially true if the depletion at the off-power condition occurs over a long exposure period. To demonstrate this capability, single assembly ANC depletion calculations were performed for each of the six lattice types at six power levels from 40% to 160% power. The k-infinity values from these calculations were compared to PARAGON assembly depletions performed at the corresponding power levels. The comparisons are presented as described below:

Tables 1-6: Full power depletions at different boron levels for each of the six fuel lattices

Tables 7-13: Off-power depletions for lattice type 1 (including restart full power depletion results)

Tables 14-18: Summary results of off-power depletions for lattice types 2 to 6

The burnup values for these tables were chosen so that, with the exception of the 0, 150, and 82000 MWD/MTU burnup points, they would be different from the burnup values used in the calculation matrix. For off-power depletions, the k-infinity comparisons for the 17x17 OFA assembly with 156 IFBA and 24 WABA are shown in detail in Tables 7 to 13. Summaries of the k-infinity results (i.e., the average difference and the maximum difference) are presented for the other assemblies in Tables 14 through 18. Note that both the average difference and the maximum difference are calculated using the absolute magnitude of the differences. [

] a,c

[

] a,c

Therefore, the results are acceptable for all lattice types at all boron concentrations, power levels and burnup steps.

Table 1 Westinghouse-type 17x17 OFA Assembly 5.0 w/o ^{235}U 156 IFBA and 24 WABA Full Power Depletions

Comparison of NEXUS/ANC to PARAGON, differences in pcm

[a,c]

Table 2 Westinghouse-type 14x14 Assembly 4.0 w/o ^{235}U 64 IFBA
Full Power Depletions

Comparison of NEXUS/ANC to PARAGON, differences in pcm

[a,c]

Table 3 Westinghouse-type 15x15 Assembly 4.5 w/o 235U 116 IFBA
Full Power Depletions

Comparison of NEXUS/ANC to PARAGON, differences in pcm

[a,c]

Table 4 CE-type 16x16 Assembly 4.2 w/o 235U with 16 Gd2O3 Burnable Absorbers
Full Power Depletions

Comparison of NEXUS/ANC to PARAGON, differences in pcm

[ ] a,c

Table 5 Westinghouse-type 17x17 Standard Assembly 4.95 w/o 235U 48 IFBA Full Power Depletions

Comparison of NEXUS/ANC to PARAGON, differences in pcm

[ ]a,c

Table 6 Westinghouse-type 17x17 OFA Assembly 2.6 w/o 235U No Burnable Absorbers Full Power Depletions

Comparison of NEXUS/ANC to PARAGON, differences in pcm

a,c

Table 7 Westinghouse-type 17x17 OFA Assembly 5.0 w/o ^{235}U 156 IFBA and 24 WABA Depletions at 40% Power

Comparison of NEXUS/ANC to PARAGON, differences in pcm

a,c

[

]

Table 8 Westinghouse-type 17x17 OFA Assembly 5.0 w/o ^{235}U 156 IFBA and 24 WABA Depletions at 60% Power

Comparison of NEXUS/ANC to PARAGON, differences in pcm

[a,c]

Table 9 Westinghouse-type 17x17 OFA Assembly 5.0 w/o ^{235}U 156 IFBA and 24 WABA Depletions at 80% Power

Comparison of NEXUS/ANC to PARAGON, differences in pcm

[a,c]

Table 10 Westinghouse-type 17x17 OFA Assembly 5.0 w/o ^{235}U 156 IFBA and 24 WABA Depletions at 100% Power

Comparison of NEXUS/ANC to PARAGON, differences in pcm

[ ]a,c

Table 11 Westinghouse-type 17x17 OFA Assembly 5.0 w/o ^{235}U 156 IFBA and 24 WABA Depletions at 120% Power

Comparison of NEXUS/ANC to PARAGON, differences in pcm

[ ]a,c

Table 12 Westinghouse-type 17x17 OFA assembly 5.0 w/o ^{235}U 156 IFBA and 24 WABA Depletions at 140% Power

Comparison of NEXUS/ANC to PARAGON, differences in pcm

[a,c]

Table 13 Westinghouse-type 17x17 OFA assembly 5.0 w/o ^{235}U 156 IFBA and 24 WABA Depletions at 160% Power

Comparison of NEXUS/ANC to PARAGON, differences in pcm

[ ] a,c

Table 14 Westinghouse-type 14x14 Assembly 4.0 w/o ^{235}U with 64 IFBA Summary of Differences: Depletions at Powers from 40% to 160%

Comparison of NEXUS/ANC to PARAGON, differences in pcm

a,c

Table 15 Westinghouse-type 15x15 Assembly 4.5 w/o ^{235}U with 116 IFBA Summary of Differences: Depletions at Powers from 40% to 160%

Comparison of NEXUS/ANC to PARAGON, differences in pcm

[a,c]

Table 16 CE-type 16x16 Assembly 4.2 w/o ^{235}U with 16 Gd_2O_3 Burnable Absorbers
Summary of Differences: Depletions at Powers from 40% to 160%

Comparison of NEXUS/ANC to PARAGON, differences in pcm

[ ]a,c

Table 17 Westinghouse-type 17x17 Standard Assembly 4.95 w/o ^{235}U with 48 IFBA Summary of Differences: Depletions at Powers from 40% to 160%

Comparison of NEXUS/ANC to PARAGON, differences in pcm

[ ]a,c

Table 18 Westinghouse-type 17x17 OFA Assembly 2.6 w/o ^{235}U No Burnable Absorbers Summary of Differences: Depletions at Powers from 40% to 160%

Comparison of NEXUS/ANC to PARAGON, differences in pcm

[a,c]

3.1.2 Zero-Power Cold Calculations

To evaluate the accuracy of calculations at zero-power cold conditions, each of the six lattice types (described in Section 3.1) were first depleted at three different RCS boron concentrations (0, 900 and 1800 ppm), then were restarted at regular depletion step intervals from 0 to 82,000 GWD/MTU, at three "cold" temperatures (68, 300, 500 ºF) and two RCS boron concentrations (0 ppm and 2600 ppm). The k-infinity results for the re-converged cold calculations are presented in Tables 19-24.

The ability to predict the eigenvalue over a wide variation in restart RCS boron concentrations and temperatures over a wide range of exposures demonstrates that the Updated NEXUS cross-section reformulation methodology is accurate for any condition that could be expected in a PWR core calculation.

The results for these cases are accurate. **[**

][a,c]

Table 19 Westinghouse-type 17x17 OFA assembly 5.0 w/o ^{235}U 156 IFBA and 24 WABA Cold Restart Reactivity Points

Comparison of NEXUS/ANC to PARAGON, differences in pcm

a,c

Table 20 Westinghouse-type 14x14 Assembly 4.0 w/o ^{235}U 64 1.5x IFBA Burnable Absorber Summary of Differences: Depletions and Cold Restart Reactivity Points

Comparison of NEXUS/ANC to PARAGON, differences in pcm

a,c

Table 21 Westinghouse-type 15x15 Assembly 4.5 w/o ^{235}U 116 1.5x IFBA Summary of Differences: Depletions and Cold Restart Reactivity Points

Comparison of NEXUS/ANC to PARAGON, differences in pcm

[ ] a,c

Table 22 CE-type 16x16 Assembly with 16 6w/o Gd_2O_3 Burnable Absorbers Summary of Differences: Depletions and Cold Restart Reactivity Points

Comparison of NEXUS/ANC to PARAGON, differences in pcm

a,c

Table 23 Westinghouse-type 17x17 standard assembly – 4.95 w/o ^{235}U 48 1.5x IFBA Summary of Differences: Depletions and Cold Restart Reactivity Points

Comparison of NEXUS/ANC to PARAGON, differences in pcm

[ ]a,c

Table 24 Westinghouse-type 17x17 OFA assembly – 2.6 w/o ^{235}U No Burnable Absorber Summary of Differences: Depletions and Cold Restart Reactivity Points

Comparison of NEXUS/ANC to PARAGON, differences in pcm

a,c

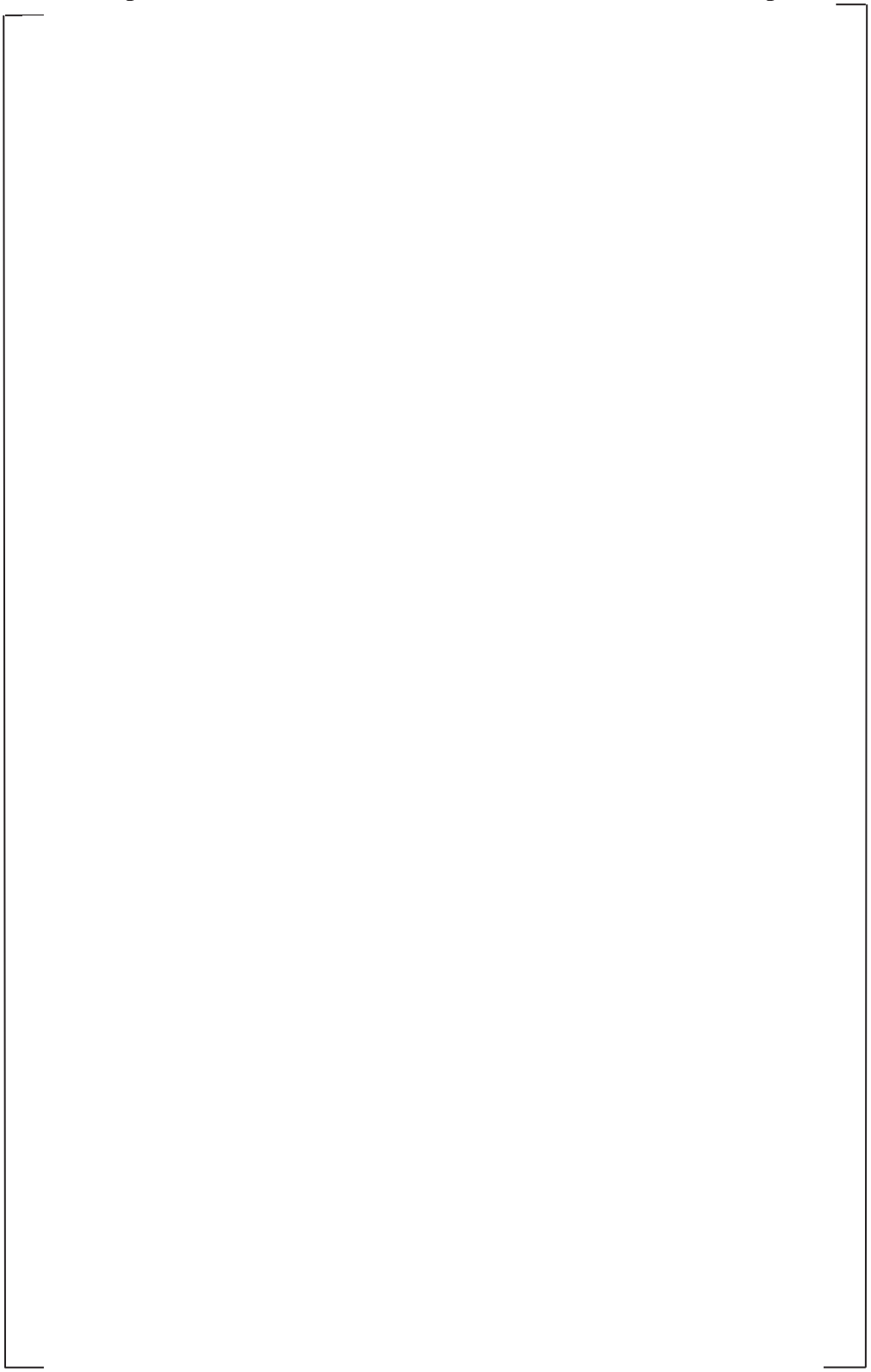

3.1.3 Calculations at Voided Conditions

The new reformulation method decouples the relationship between moderator temperature and moderator density, giving excellent results at off-nominal voided conditions where local moderator density is changed due potentially to a combination of system depressurization and high local power (similar to conditions present during a steamline break event). To demonstrate the efficacy of this decoupling, the fuel assembly depletions at the three RCS boron concentrations described in Section 3.1.2 were re-converged at multiple depletion steps with a wide range of void fractions (-2%, 5%, 15%, 25%, and 40%), each at two soluble boron concentrations (0 and 2600 ppm). Negative void fraction represents the case with the condition of core pressure increment. Table 25 presents the k-infinity comparisons in detail for the 17x17 OFA assembly with 156 IFBA and 24 WABA, while Tables 26 to 30 summarize the comparisons for the other five fuel lattice types described in Section 3.1.

The results for these cases are accurate over the range of void fraction analyzed. **[**

] [a,c] The accuracy of the k-infinity prediction is maintained, even with the increment of void fraction.

Table 25 Westinghouse-type 17x17 OFA assembly 5.0 w/o ^{235}U 156 IFBA and 24 WABA Restart Reactivity Points for Voided Conditions

Comparison of NEXUS/ANC to PARAGON, differences in pcm

a,c

Table 25: Westinghouse-type 17x17 OFA assembly 5.0 w/o ^{235}U 156 IFBA and 24 WABA Restart Reactivity Points for Voided Conditions (cont.)

Comparison of NEXUS/ANC to PARAGON, differences in pcm

a,c

Table 26 Westinghouse-type 14x14 Assembly with 64 IFBA Burnable Absorbers Summary of Differences: Restart Reactivity Points for Voided Conditions

Comparison of NEXUS/ANC to PARAGON, differences in pcm

[ ] a,c

Table 27 Westinghouse-type 15x15 Assembly with 116 IFBA Burnable Absorbers Summary of Differences: Restart Reactivity Points for Voided Conditions

Comparison of NEXUS/ANC to PARAGON, differences in pcm

[ ] a,c

Table 28 CE-type 16x16 Assembly with 16 6w/o Gd_2O_3 Burnable Absorbers Summary of Differences: Restart Reactivity Points for Voided Conditions

Comparison of NEXUS/ANC to PARAGON, differences in pcm

[ ]a,c

Table 29 Westinghouse-type 17x17 Standard Assembly – 4.95 w/o ^{235}U 48 IFBA Summary of Differences: Restart Reactivity Points for Voided Conditions

Comparison of NEXUS/ANC to PARAGON, differences in pcm

[ ] a,c

Table 30 Westinghouse-type 17x17 OFA assembly – 2.6 w/o ^{235}U No Burnable Absorber Summary of Differences: Restart Reactivity Points for Voided Conditions

Comparison of NEXUS/ANC to PARAGON, differences in pcm

[ ]a,c

3.1.4 Evaluation of New Cross-Section Reformulation Methods on Pin Power Distribution

In Reference 3, Westinghouse developed an advanced pin power calculation methodology which was implemented in the NEXUS/ANC code system. The fundamental pin power calculation methodology remains the same for the updated NEXUS/ANC methodology except for the pin cell cross-sections, which will use the new cross-section reformulation instead.

The impact of the pin cell cross-section model on pin power calculation results was analyzed by performing single assembly pin power calculations and directly comparing the results between the new cross-section reformulation and the currently licensed NEXUS/ANC. The lattice type 5, illustrated in Figure 1, was modeled and analyzed in this report.

Figure 1 Map of Westinghouse 17x17 Standard Rod Size Assembly – 4.95 w/o 235U 48 IFBA

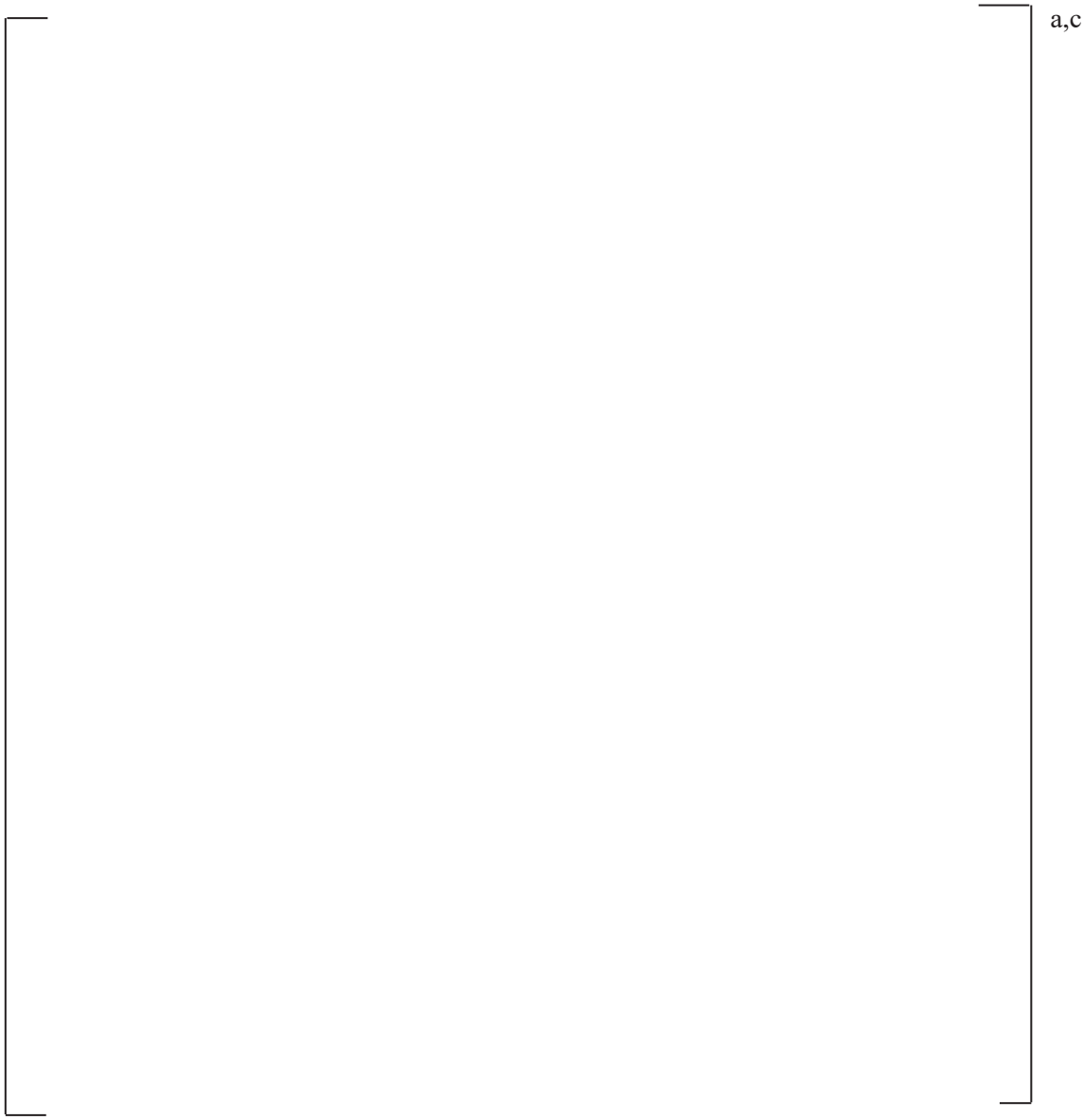

The fuel assembly was depleted at both unrodded and rodded conditions. For the unrodded case, Figure 2 shows the pin power distribution difference for the up-left quadrant of the assembly at 20,000 MWD/MTU. The difference is defined as the new cross-section reformulation value minus the value using the current NEXUS/ANC methodology.

Figure 2 Pin Power Difference at 20,000 MWD/MTU for Unrodded Case

0.003	0.002	0.003	0.001	0.001	0.001	0.001	0.001	0.001
0.002	0.002	0.001	0.000	0.000	-0.001	0.000	0.000	-0.001
0.003	0.001	0.000	-0.001	-0.002		0.000	-0.001	
0.001	0.000	0.000		-0.002	-0.001	0.000	0.000	0.000
0.001	0.000	-0.002	-0.002	0.000	-0.002	0.000	0.000	-0.001
0.001	-0.001		-0.001	-0.002		0.000	-0.001	
0.001	0.000	0.000	0.000	0.000	0.000	0.000	0.001	0.000
0.001	0.000	-0.001	0.000	0.000	-0.001	0.001	0.001	0.000
0.001	-0.001		0.000	-0.001		0.000	0.000	

For the rodded case, two insertion scenarios for the Ag-In-Cd black control rods as shown in Figure 3, in which the control rods are fully inserted and withdrawn at various depletion intervals.

Figure 3 Illustration of Control Rods Insertion Scenarios

a,c

Throughout the depletion history, both the assembly maximum power (F_Q) and pin (5,4) power were evaluated. Fuel pin (5,4) was chosen because it is next to a guide thimble where the control rod strongly impacts the power of that pin. Figures 4 to 7 show the impact of the cross-section methodology change on F_Q and pin (5,4) power for both control rod insertion scenarios. Figures 8 and 9 show the detailed comparison of the pin power distribution at 12000 MWD/MTU.

The results demonstrate that adopting the new cross-section reformulation in the pin-cell cross-section calculation has no impact on the pin power calculation, as desired. The maximum change of the pin power is approximately 1%. Therefore, the licensed ANC pin power reconstruction methodology **[**Reference 3**]** continues to function appropriately with the new cross-section methodology.

Figure 4 Impact of Cross-Section Model on Fq for CR Sequence 1

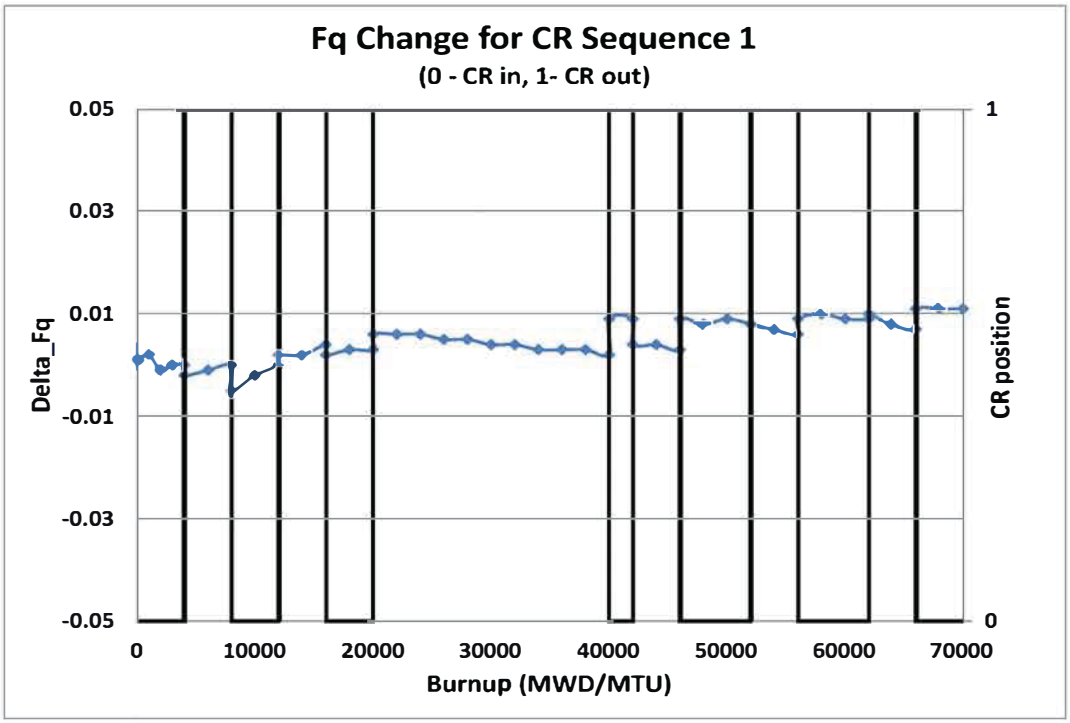

Figure 5 Impact of Cross-Section Model on Power Distribution of Pin (5,4) for Sequence 1

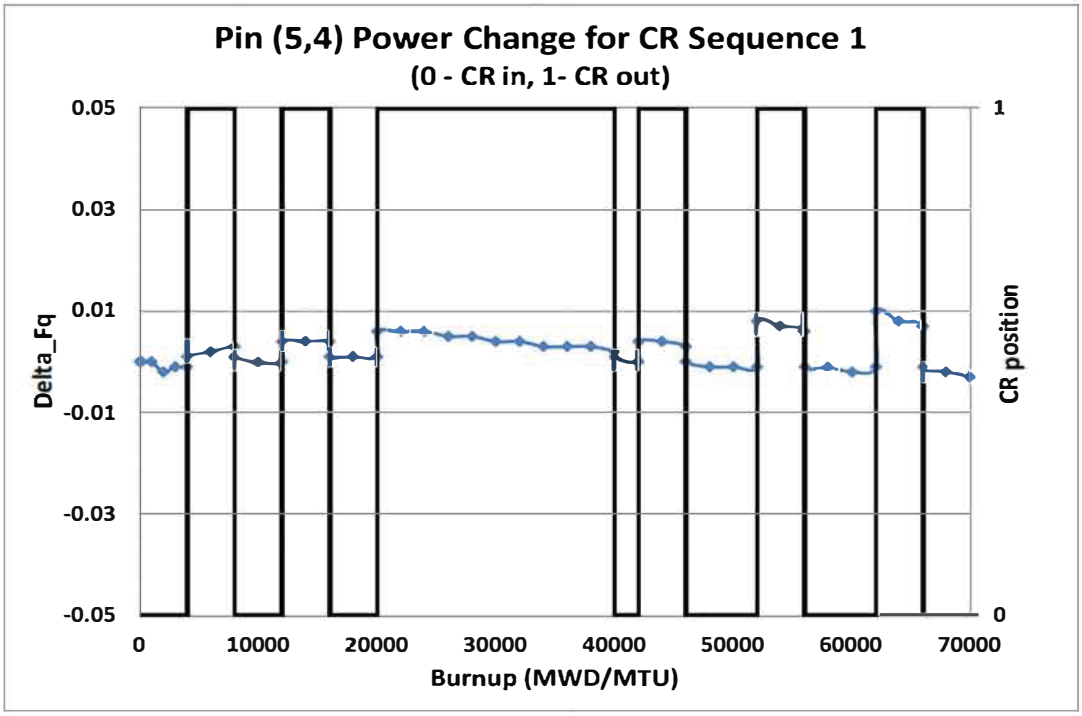

Figure 6 Impact of Cross-Section Model on FQ or CR Sequence 2

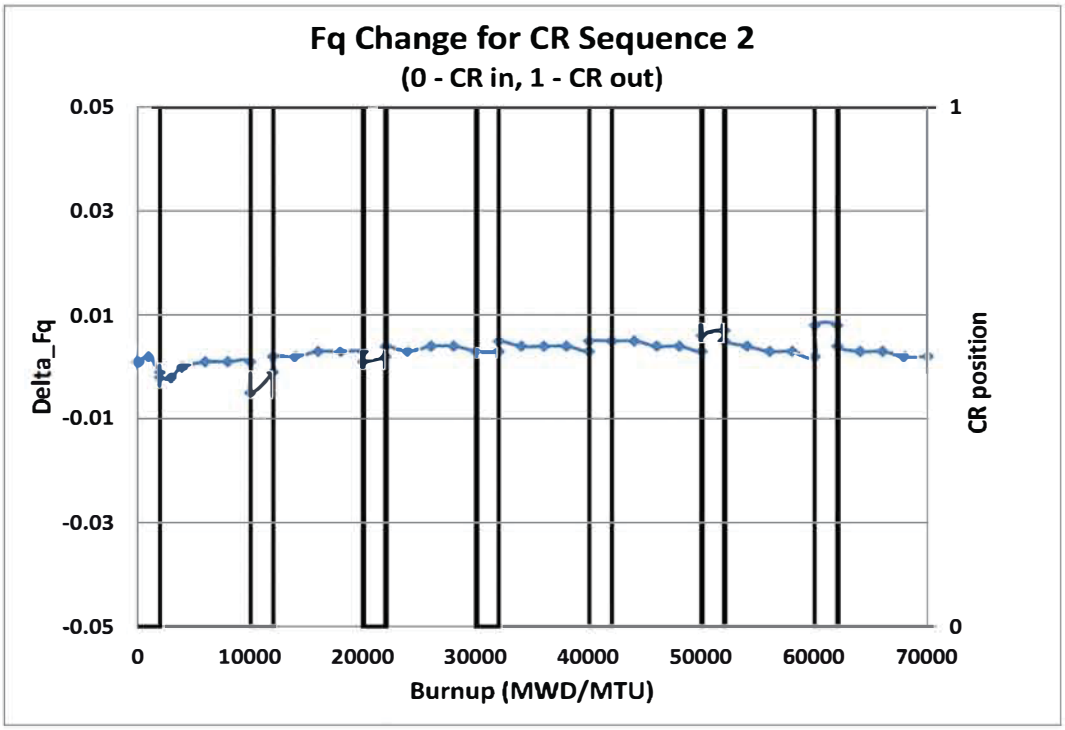

Figure 7 Impact of Cross-Section Model on Power Distribution of Pin (5,4) for Sequence 2

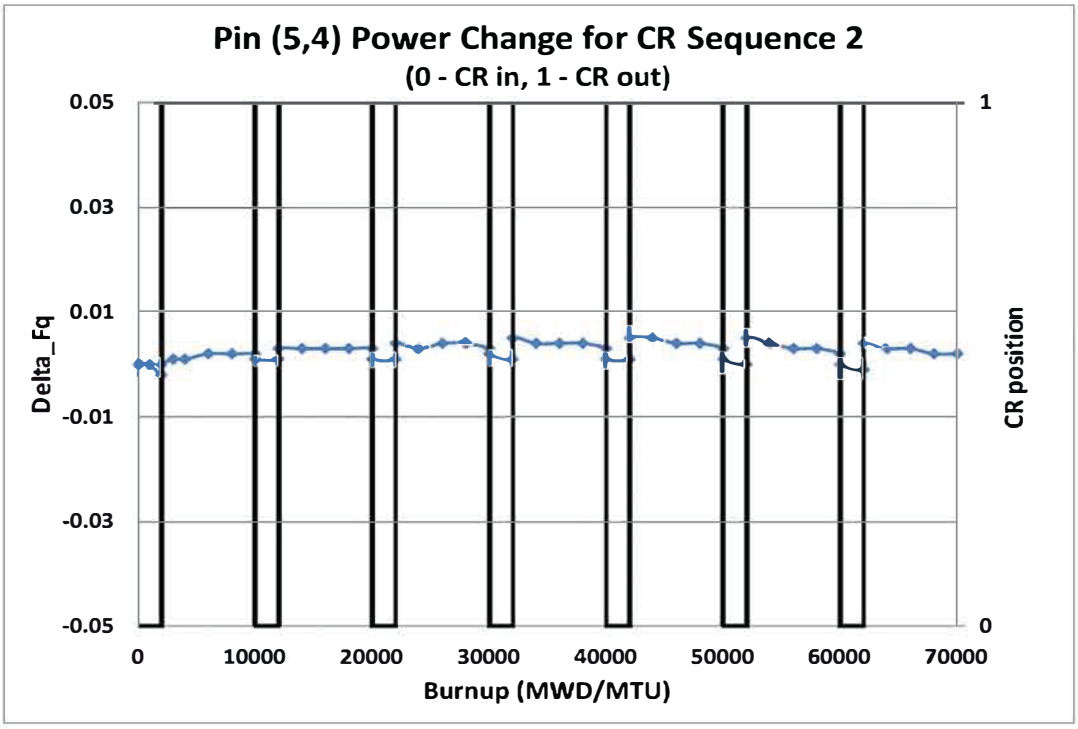

Figure 8 Pin Power Difference at 12000 MWD/MTU for Scenario 1

0.000	0.001	0.000	-0.001	-0.001	-0.001	-0.001	-0.001	0.000
0.001	0.000	-0.001	-0.001	-0.001	0.000	-0.001	0.000	0.000
0.000	-0.001	-0.001	0.000	-0.001		0.000	-0.001	
-0.001	-0.001	0.000		0.000	0.001	0.001	0.001	0.001
-0.001	-0.001	-0.001	0.000	0.001	0.000	0.001	0.001	0.001
-0.001	0.000		0.001	0.000		0.002	0.000	
-0.001	-0.001	0.000	0.001	0.001	0.002	0.000	0.000	0.000
-0.001	0.000	-0.001	0.001	0.001	0.000	0.000	0.000	-0.002
0.000	0.000		0.001	0.001		0.000	-0.002	

Figure 9 Pin Power Difference at 12000 MWD/MTU for Scenario 2

0.001	0.002	0.000	0.000	-0.001	0.000	0.000	0.000	0.000
0.002	0.000	0.000	-0.001	-0.001	-0.001	-0.001	0.000	0.000
0.000	0.000	-0.001	0.000	-0.001		0.000	-0.001	
0.000	-0.001	0.000		-0.001	0.001	0.001	0.000	0.001
-0.001	-0.001	-0.001	-0.001	0.000	0.000	0.001	0.001	0.001
0.000	-0.001		0.001	0.000		0.000	0.000	
0.000	-0.001	0.000	0.001	0.001	0.000	0.000	0.000	0.000
0.000	0.000	-0.001	0.000	0.001	0.000	0.000	0.000	-0.001
0.000	0.000		0.001	0.001		0.000	-0.001	

3.2 MINICORE MODEL CALCULATIONS

Due to the strong interaction between MOX and UO_2 fuel assemblies, it has been a challenge for traditional core design methods to model UO_2-MOX mixed cores. To evaluate the impact of the re-homogenization methods, a 3x3 UO_2-MOX checker-board mini-core case was setup with 5 MOX (M) and 4 UO_2 (U) fuel assemblies. The configuration of the mini-core case is given in Figure 10. The reflective boundary condition is applied to the outer surface of the mini-core system.

Figure 10 Configuration of 3x3 Mini-Core

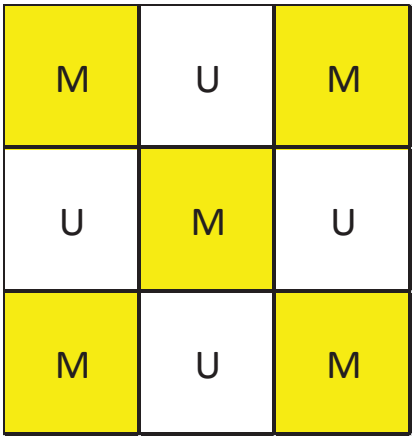

NEXUS/ANC calculations were performed with and without the re-homogenization model, while a PARAGON calculation was performed with the same geometry to generate reference results. The k_∞ comparison of NEXUS/ANC predictions against the reference is given in Table 31, while Figure 11 shows the comparison of assembly power distribution.

The re-homogenization model captures the interaction effect between the dissimilar fuel assemblies and improves the prediction on both the reactivity and assembly power distribution.

Table 31 Comparison of k_∞ for 3X3 Mini-Core Case

[ ] a,c

Figure 11 Comparison of Assembly Power Comparison for Mini-Core Case

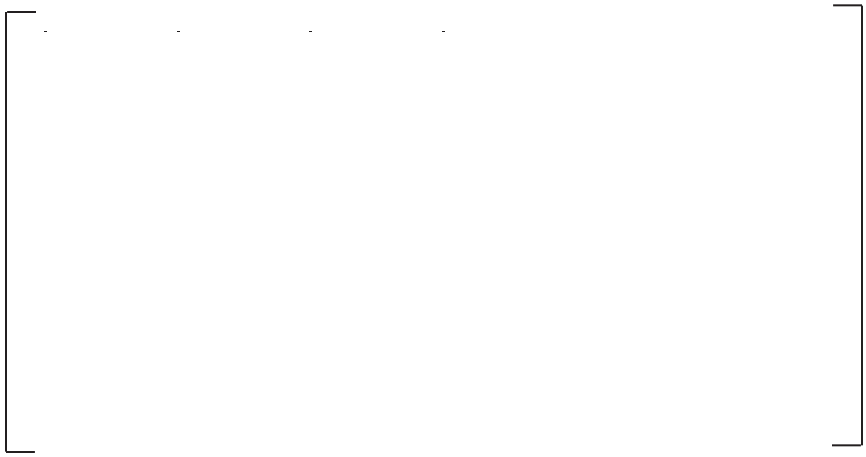
a,c

3.3 PWR CORE CALCULATIONS

Core models were generated using both the currently licensed and the updated NEXUS/ANC methodologies to demonstrate the accuracy of the updated NEXUS/ANC system for actual core calculations. Core models representing previously operated cycles were set up for four plants:

Plant A: Combustion Engineering plant: 217 assembly core, 16x16 lattice. Cycles 11, 12, 13, and 14 are modeled. Burnable absorber is Gd_2O_3 for all modeled cycles.

Plant B: Westinghouse plant: 193 assembly core (4 loops), 17x17 OFA lattice. Cycles 8, 9, 10, 11, 12 are modeled. Burnable absorber for all cycles is IFBA.

Plant C: Westinghouse plant: 157 assembly core (3 loops), 17x17 standard lattice. Cycles 18, 19, and 20 are modeled. Burnable absorber for all cycles is IFBA.

Plant D: The Westinghouse **AP1000®** Plant: 157 assembly core, 17x17 lattice. First cycle. Burnable absorbers are WABA and IFBA.

In addition to modeling these actual plant cycles, an equilibrium cycle model was set up based on a Westinghouse 4 loop 17x17 core with standard size fuel rods. This model was set up using both the currently licensed NEXUS/ANC9 method and the updated NEXUS/ANC method to compare power distributions, rodworths, and cold critical boron calculations.

3.3.1 At-Power Critical Boron Results

Figures 12 through 23 present the comparisons of the currently licensed and the updated NEXUS/ANC results against measured data for at-power RCS critical boron concentration versus cycle burnup. **[**

][a,c] Note that adjustments to the measured data to account for B depletion were not included in any of these calculations although it is clearly in evidence in several of the cycles.

3.3.2 At-Power Axial Offset Results

Table 32 gives the axial offset (AO) comparison as a function of cycle burnup for cycles 18 through 20 of Plant C. **[**

] a,c

3.3.3 Startup Test Physics Predictions

Tables 33 and 34 show the comparison of low power physics test results (i.e., measured values) against predictions from both the currently licensed and updated NEXUS/ANC models for cycles 18 through 20 for Plant C and the first cycle of Plant D. The comparison was made to the available measurement data such as hot zero power (HZP), all rods out (ARO) critical boron, HZP ARO isothermal temperature coefficient (ITC), HZP ARO moderator temperature coefficient (MTC), and HZP ARO boron worth.

[

] a,c

3.3.4 Power Distributions

Comparisons of radial power distributions between currently licensed and updated NEXUS/ANC are shown in Figures 24-29 for the equilibrium cycle core described above. Both assembly power and peak rod power are compared at three times in life: Beginning of Cycle (BOC) (0 MWD/MTU), Middle of Cycle (MOC) (10000 MWD/MTU) and at End of Cycle (EOC) (21436 MWD/MTU).

[

] a,c

3.3.5 Rod Worths

Rod worth comparisons between the currently licensed and updated NEXUS/ANC were performed with the equilibrium cycle models. The results are shown in Table 35 for BOC, MOC, and EOC. **[**

] a,c

3.3.6 Cold Reactivity Calculations

Table 36 provides comparisons of critical boron concentrations at 68°F, 200°F, and 350°F for all control rods out (ARO), all control rods in (ARI) and with all rods in but the most reactive rod (ARI-1) for BOC, MOC, and EOC of the equilibrium cycle models. The table shows the reactivity difference between both models in ppm and the rod worth of the ARI and ARI-1 cases.
[

] a,c

Figure 12 Plant A Cycle 11
Critical Boron Concentration versus Cycle Burnup

a,b,c

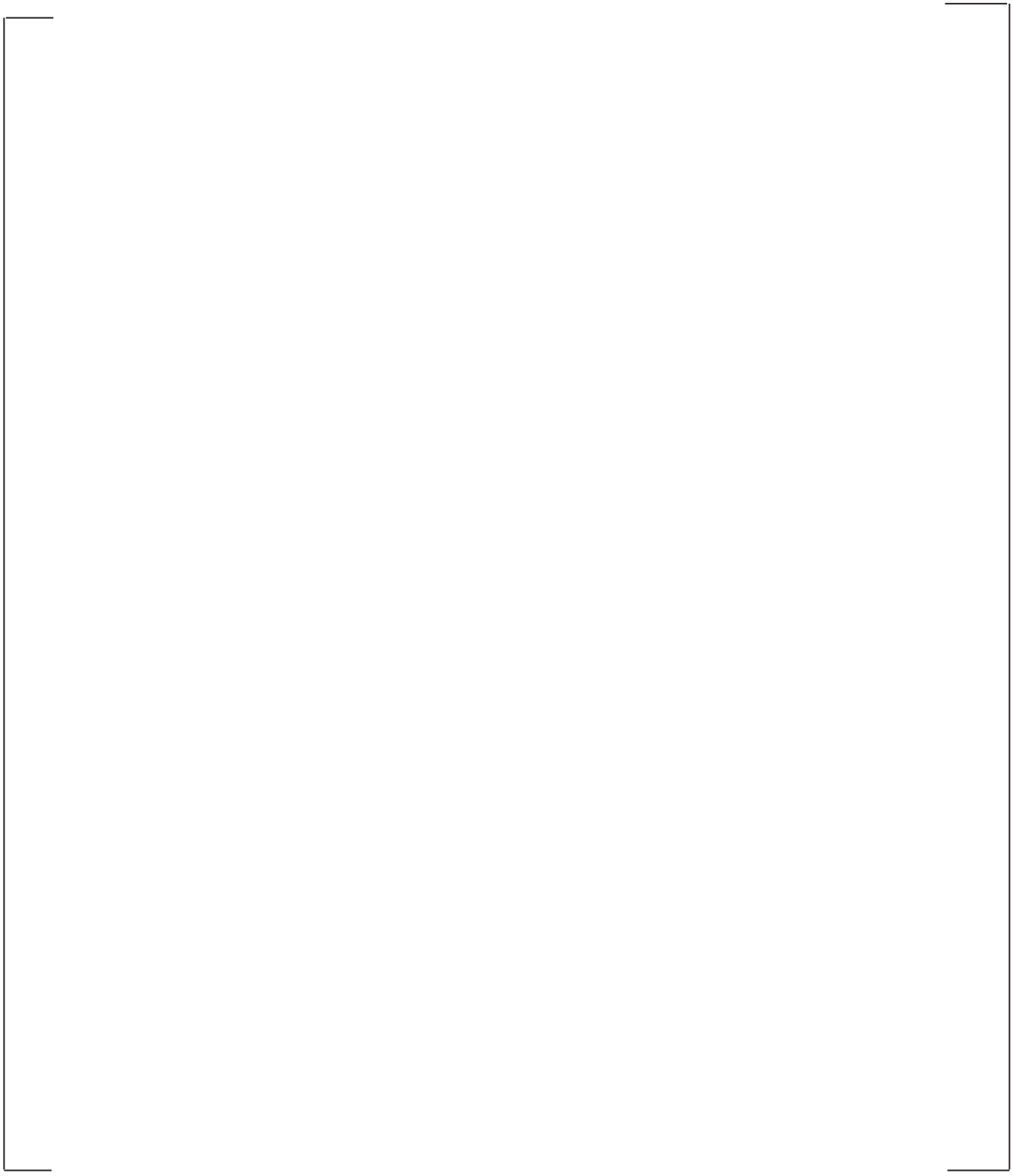

Figure 13 Plant A Cycle 12
Critical Boron Concentration versus Cycle Burnup

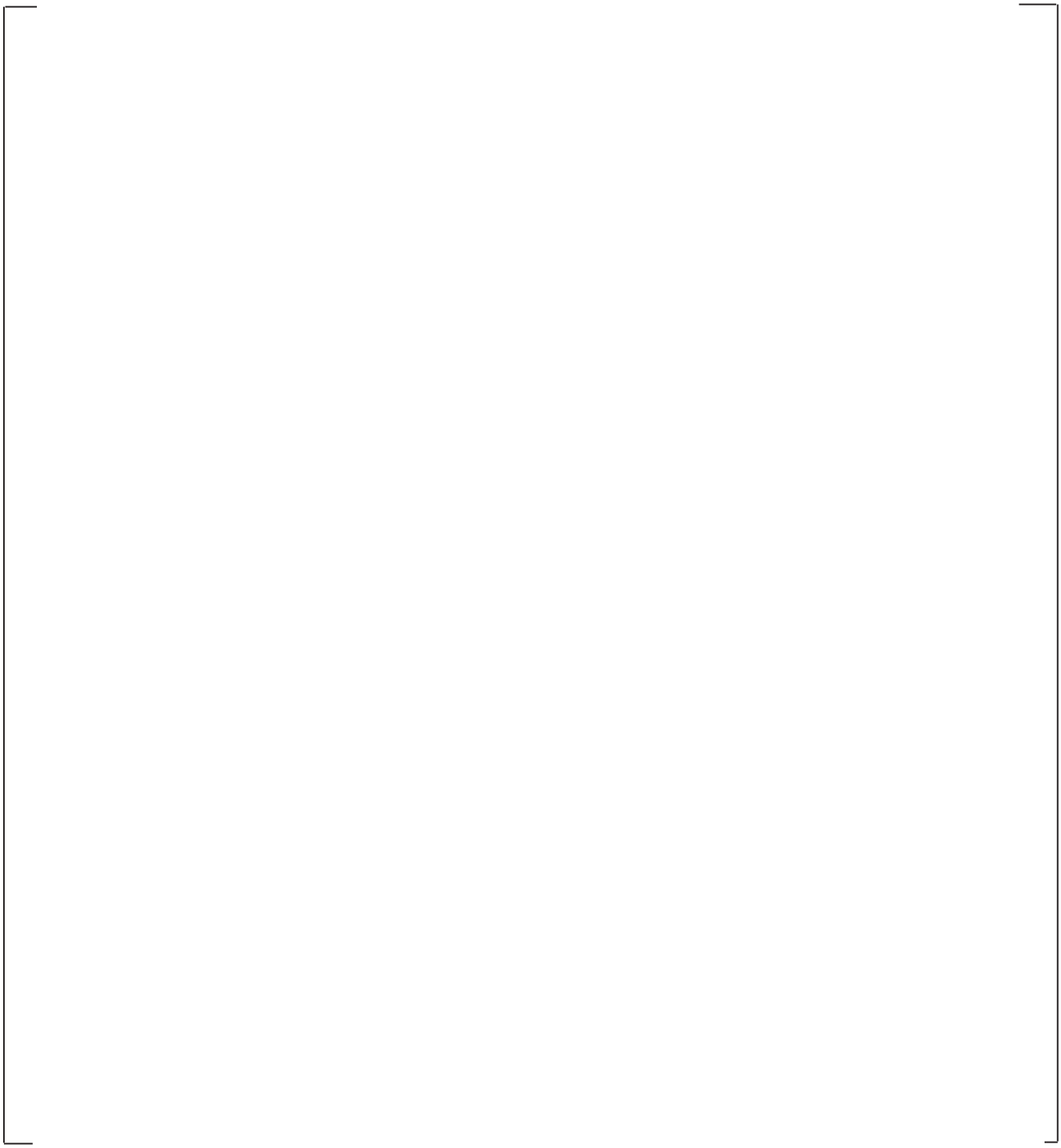

a,b,c

Figure 14 Plant A Cycle 13
Critical Boron Concentration versus Cycle Burnup

a,b,c

Figure 15 Plant A Cycle 14
Critical Boron Concentration versus Cycle Burnup

a,b,c

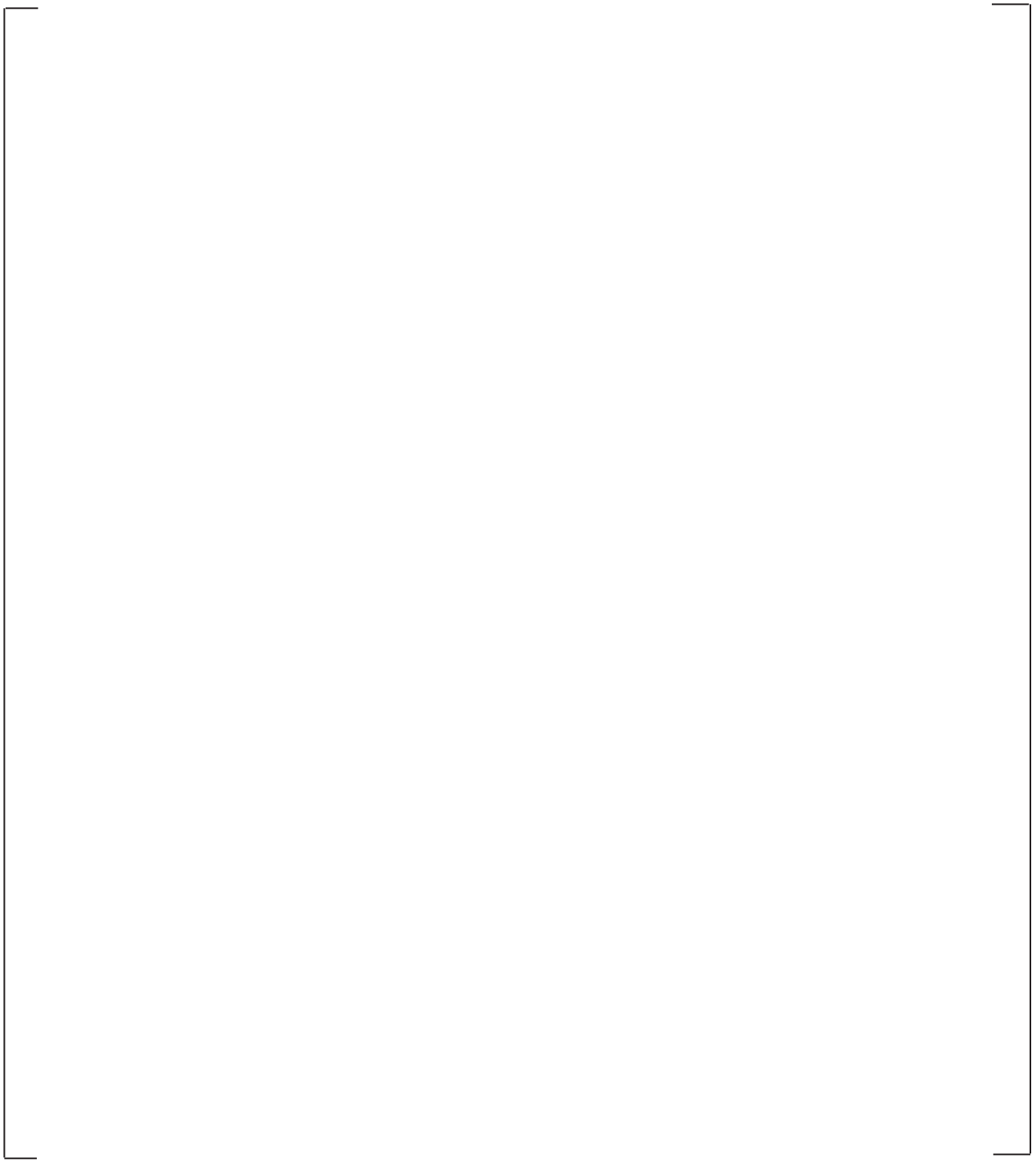

Figure 16 Plant B Cycle 8
Critical Boron Concentration versus Cycle Burnup

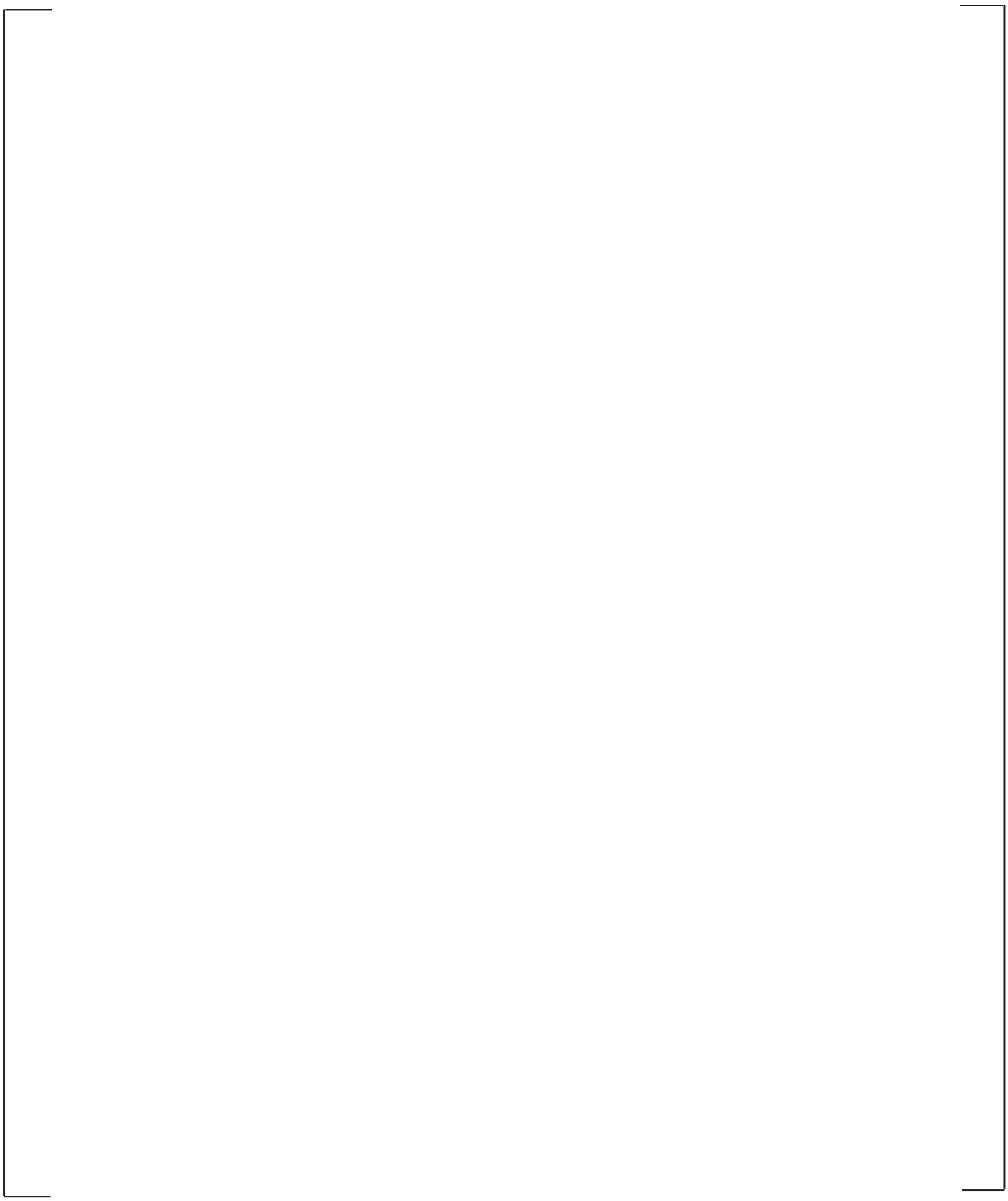

a,b,c

Figure 17 Plant B Cycle 9
Critical Boron Concentration versus Cycle Burnup

a,b,c

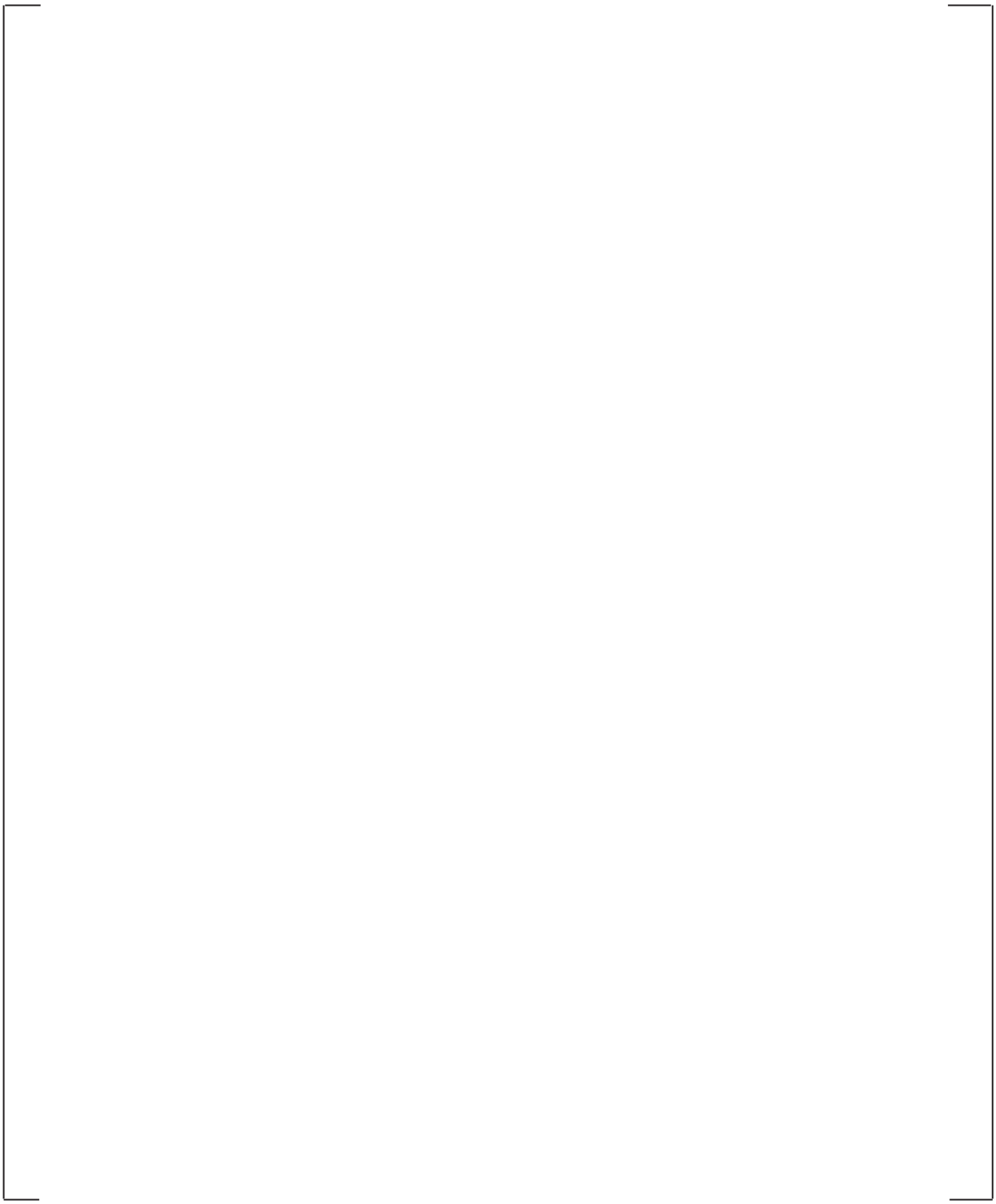

Figure 18 Plant B Cycle 10
Critical Boron Concentration versus Cycle Burnup

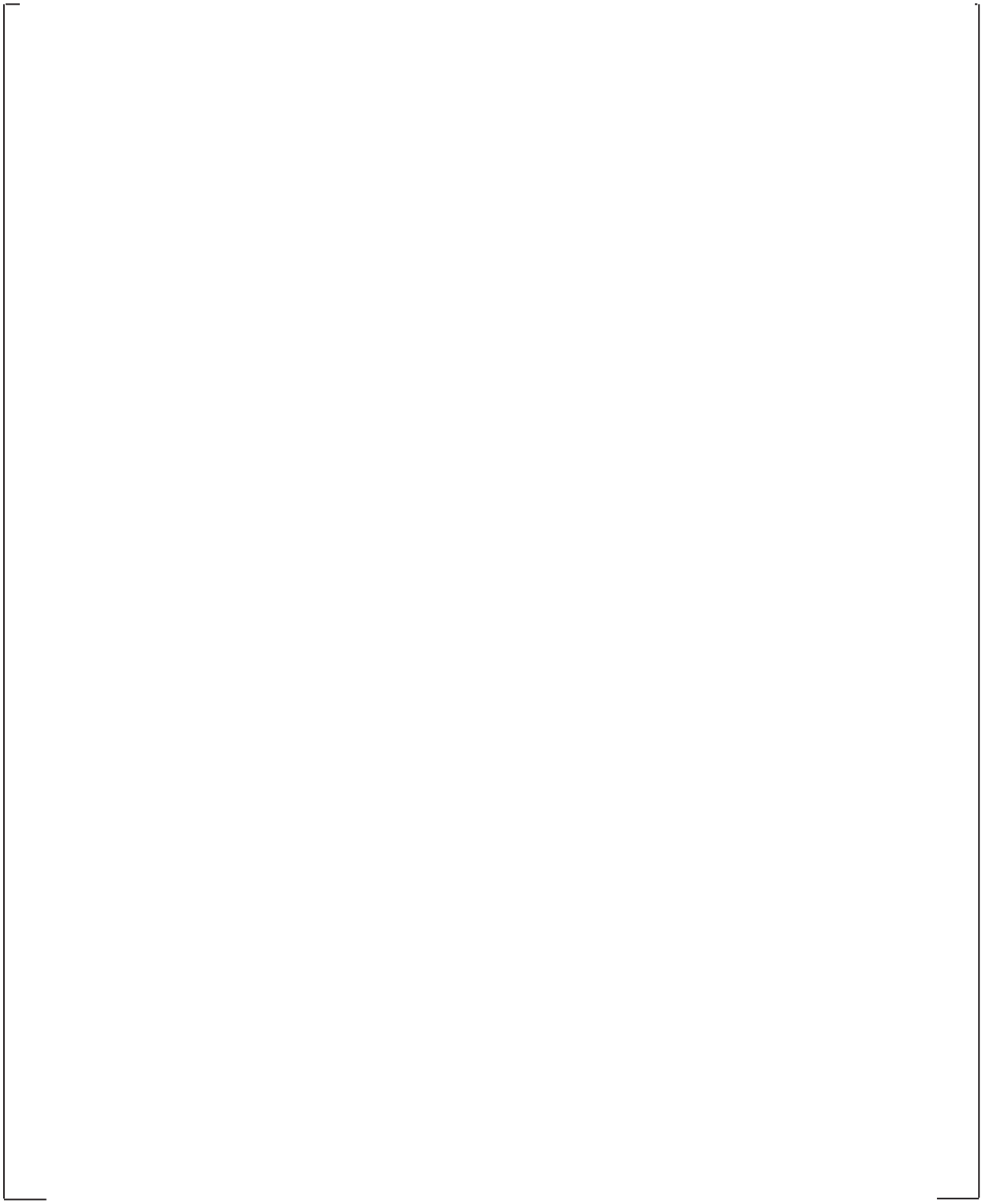

a,b,c

Figure 19 Plant B Cycle 11
Critical Boron Concentration versus Cycle Burnup

a,b,c

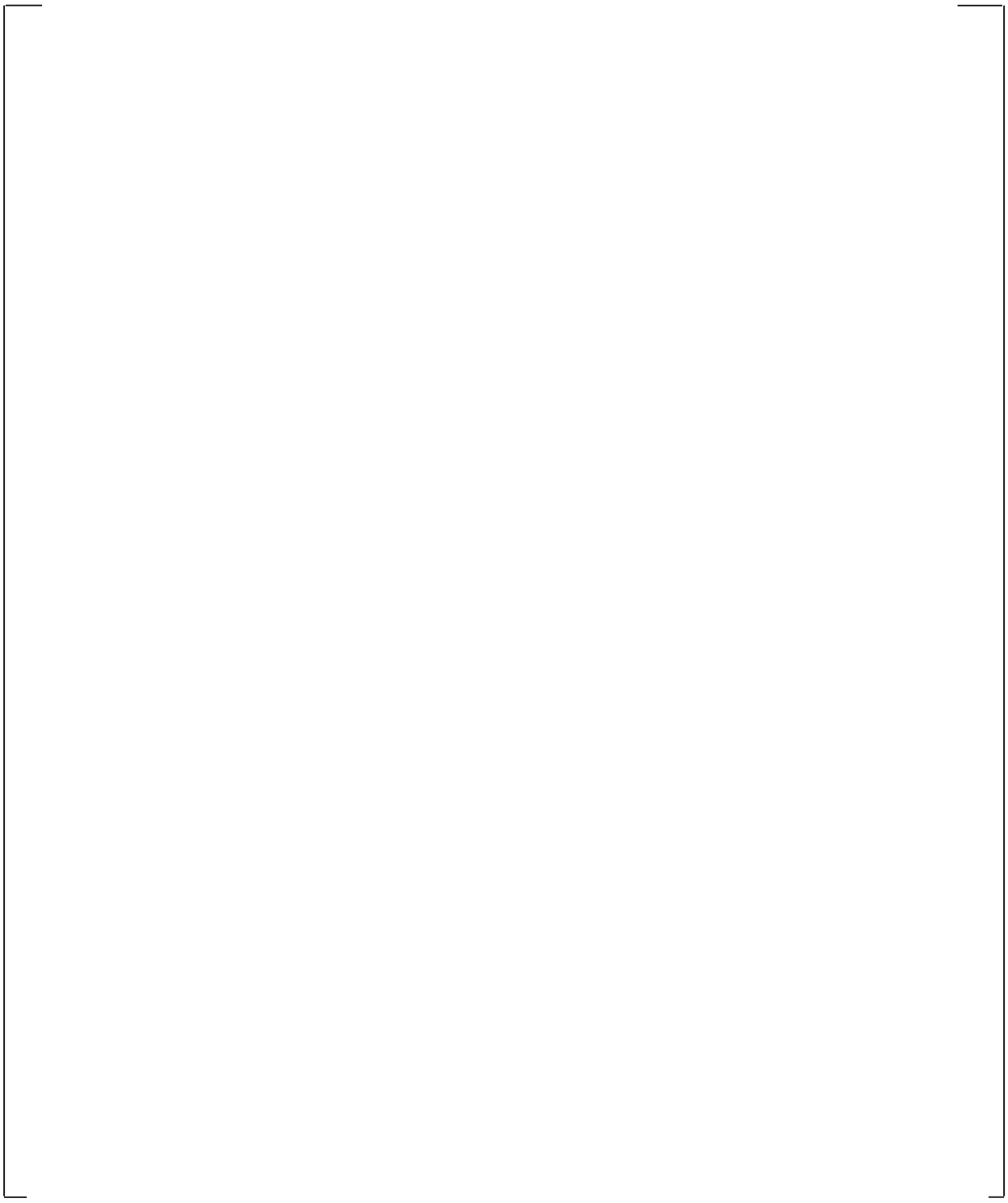

Figure 20 Plant B Cycle 12
Critical Boron Concentration versus Cycle Burnup

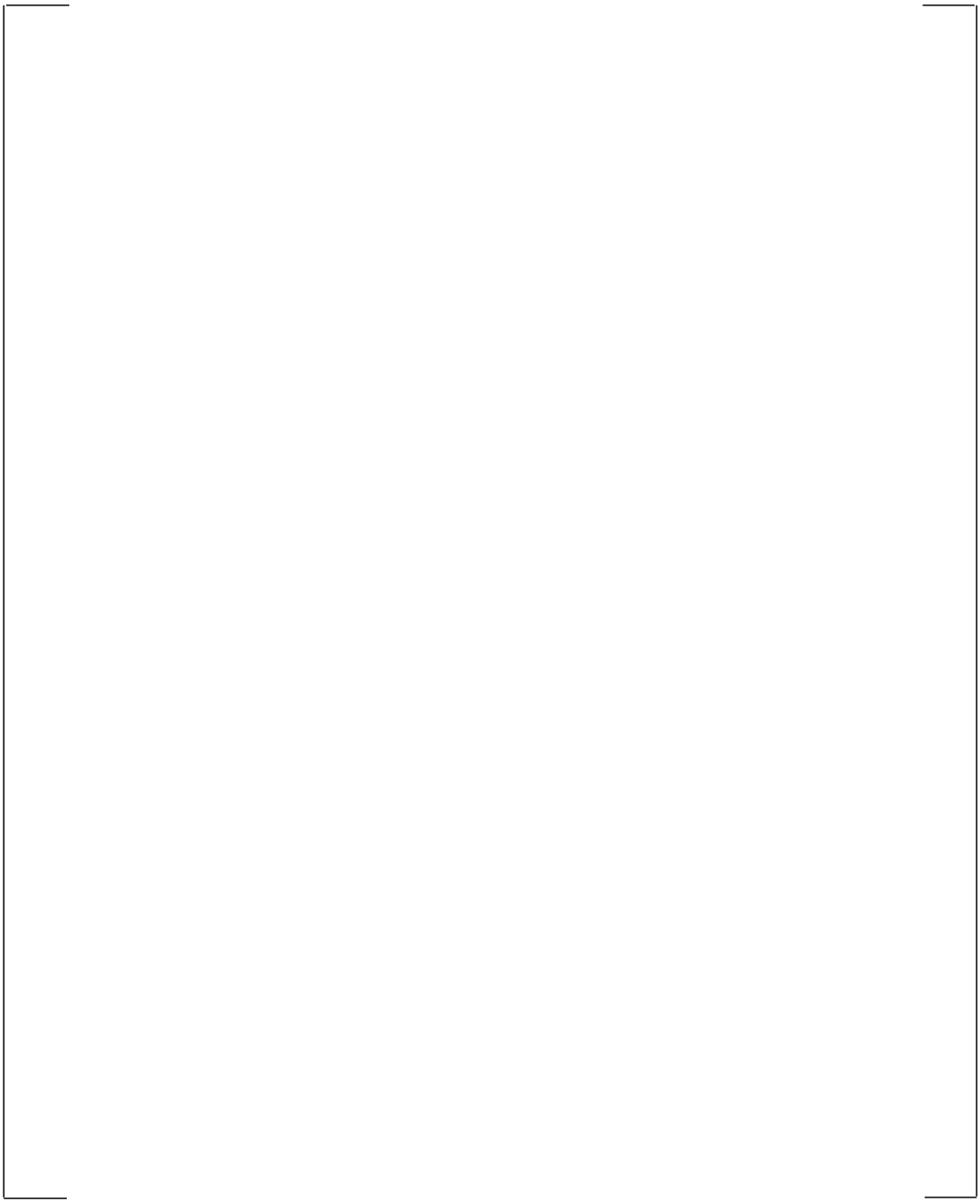

a,b,c

Figure 21 Plant C Cycle 18
Critical Boron Concentration versus Cycle Burnup

a,b,c

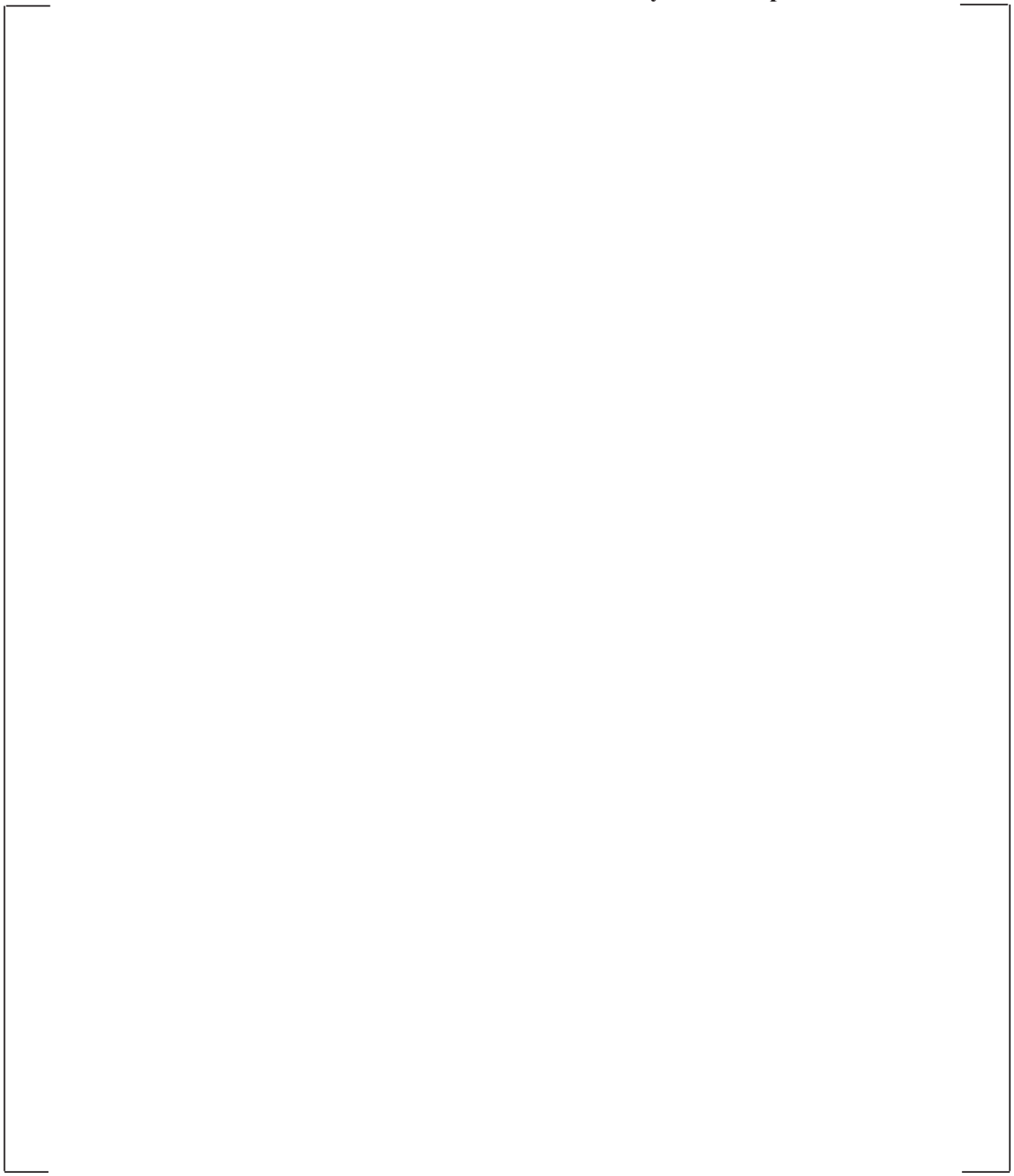

Figure 22 Plant C Cycle 19
Critical Boron Concentration versus Cycle Burnup

a,b,c

Figure 23 Plant C Cycle 20
Critical Boron Concentration versus Cycle Burnup

a,b,c

Table 32 Plant C Axial Offset versus Cycle Burnup

a,b,c

Table 33 Plant C Low Power Physics Test Data

[a,b,c]

Table 34 Plant D First Cycle Startup Low Power Physics Test Data

[a,b,c]

Figure 24 Equilibrium Cycle BOC Assembly Power Distribution New versus Current NEXUS/ANC

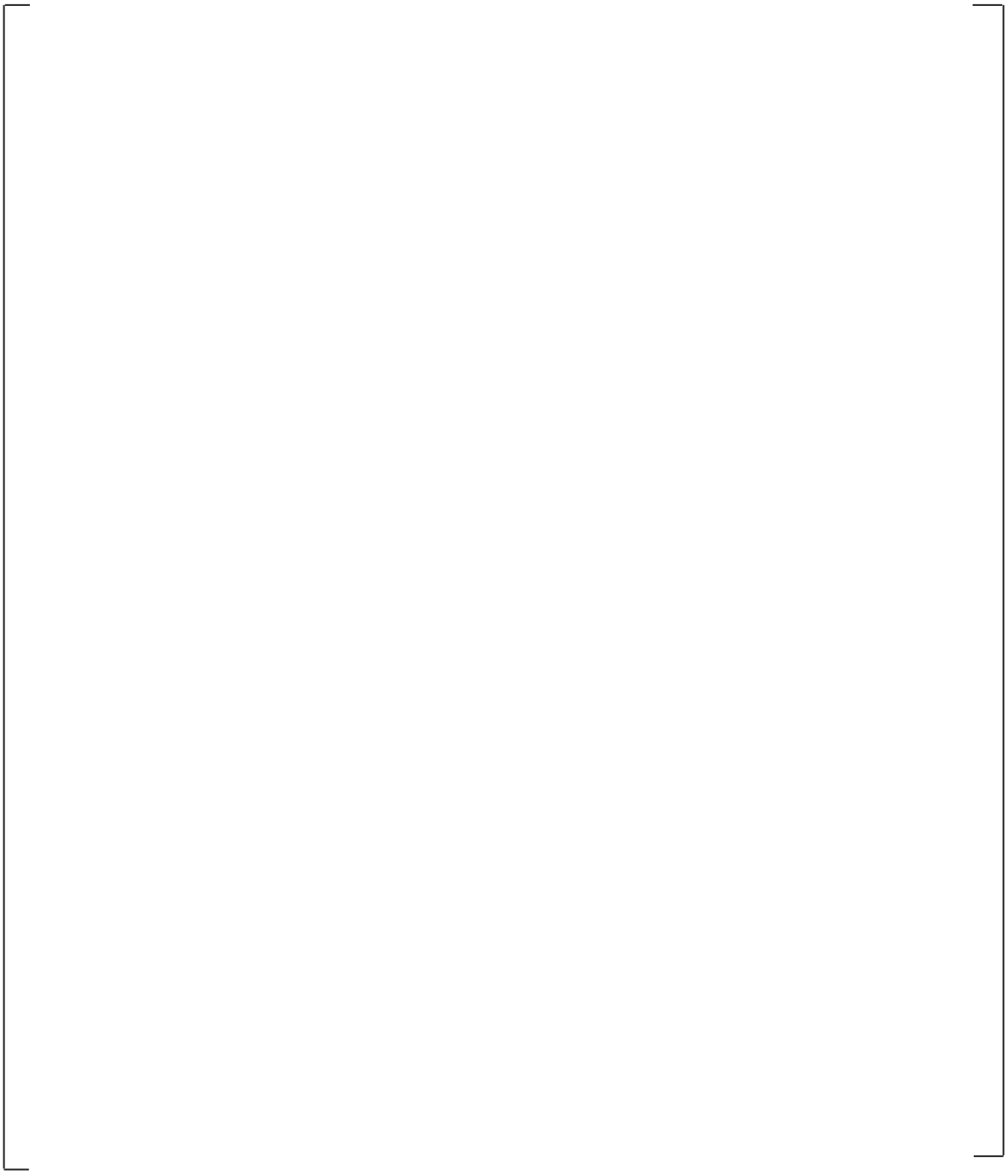

a,c

Figure 25 Equilibrium Cycle MOC Assembly Power Distribution New versus Current NEXUS/ANC

a,c

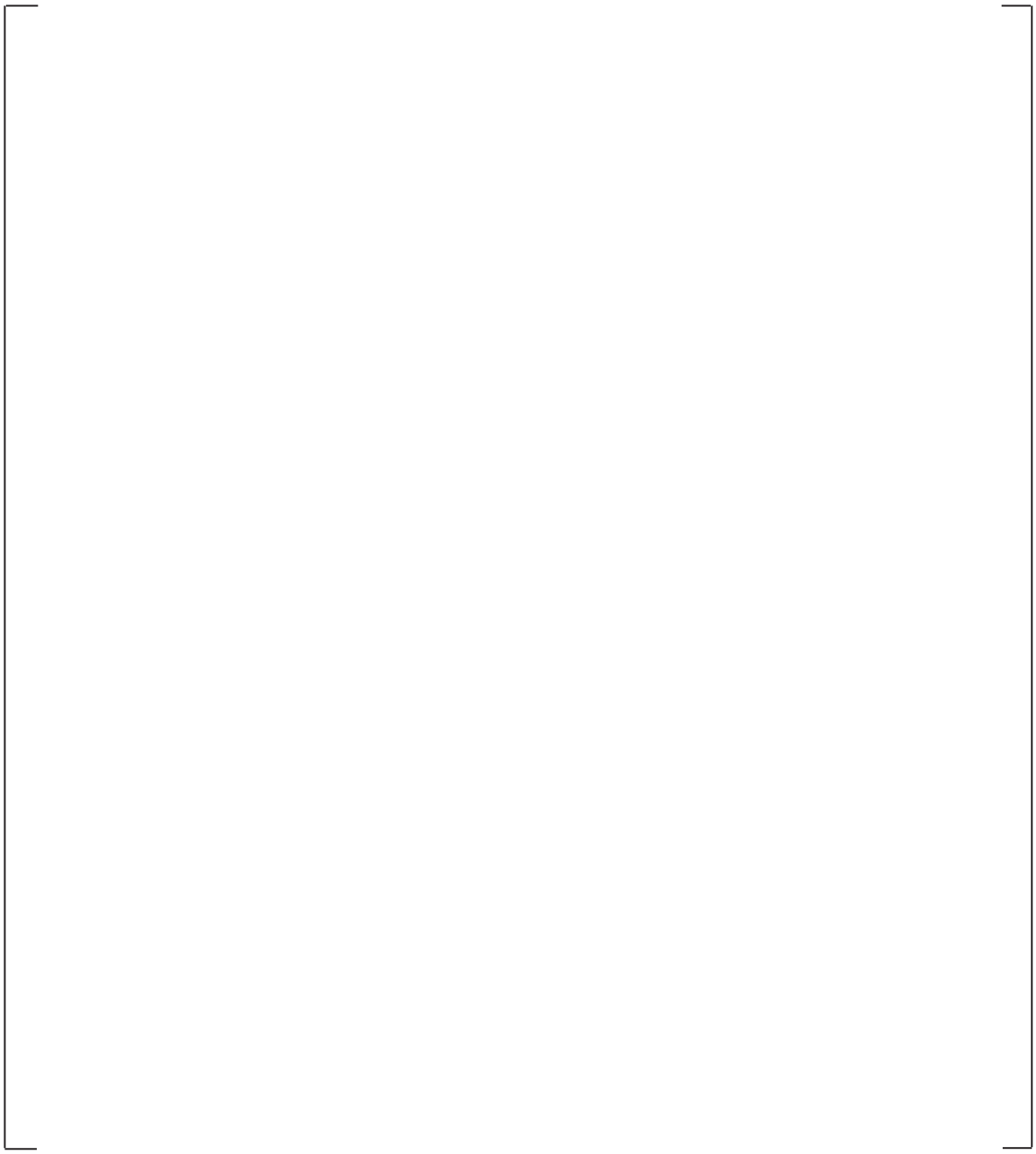

Figure 26 Equilibrium Cycle EOC Assembly Power Distribution New versus Current NEXUS/ANC

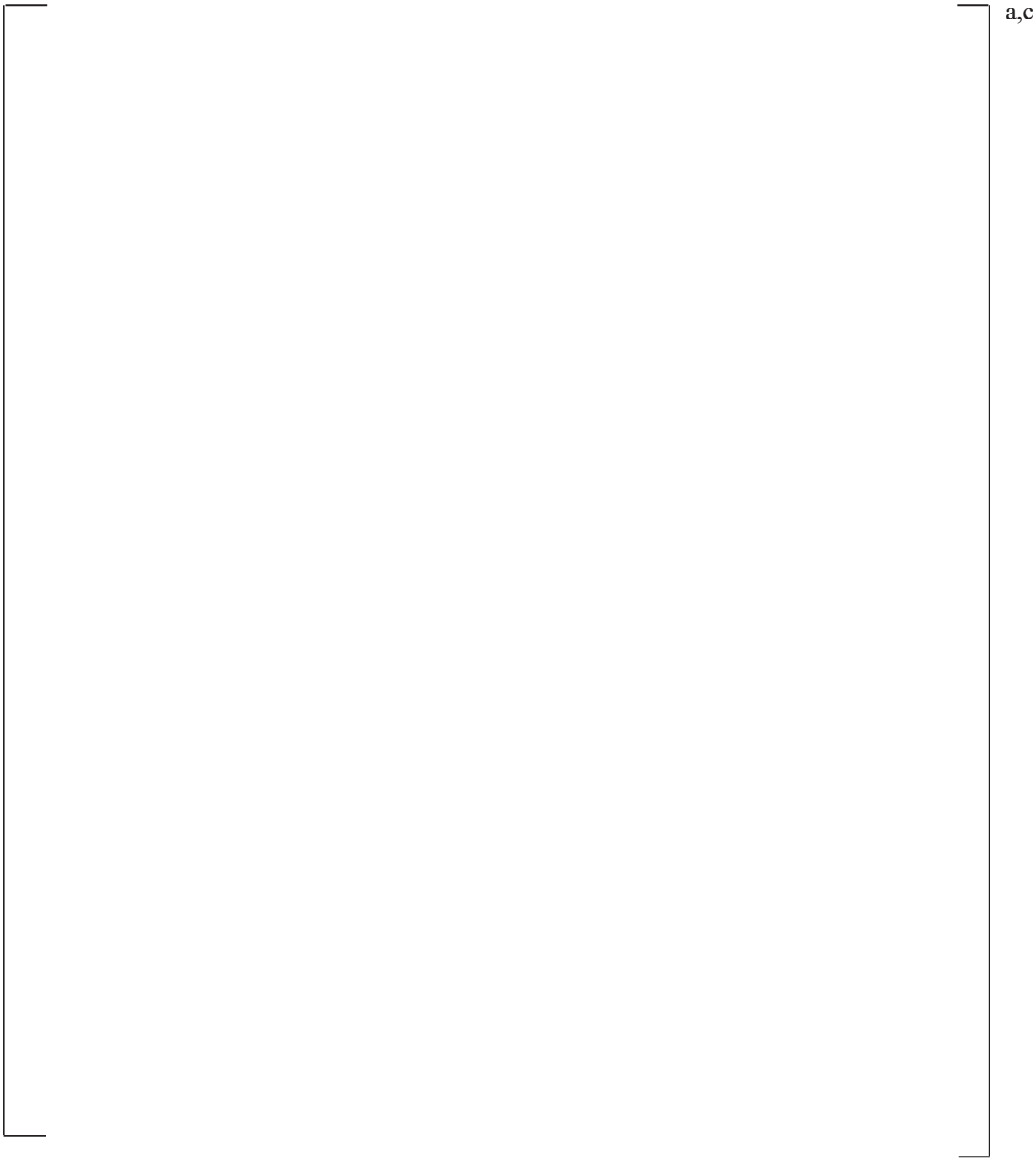

a,c

Figure 27 Equilibrium Cycle BOC Radial Peaking Factor ($F_{\Delta H}$) Distribution New versus Current NEXUS/ANC

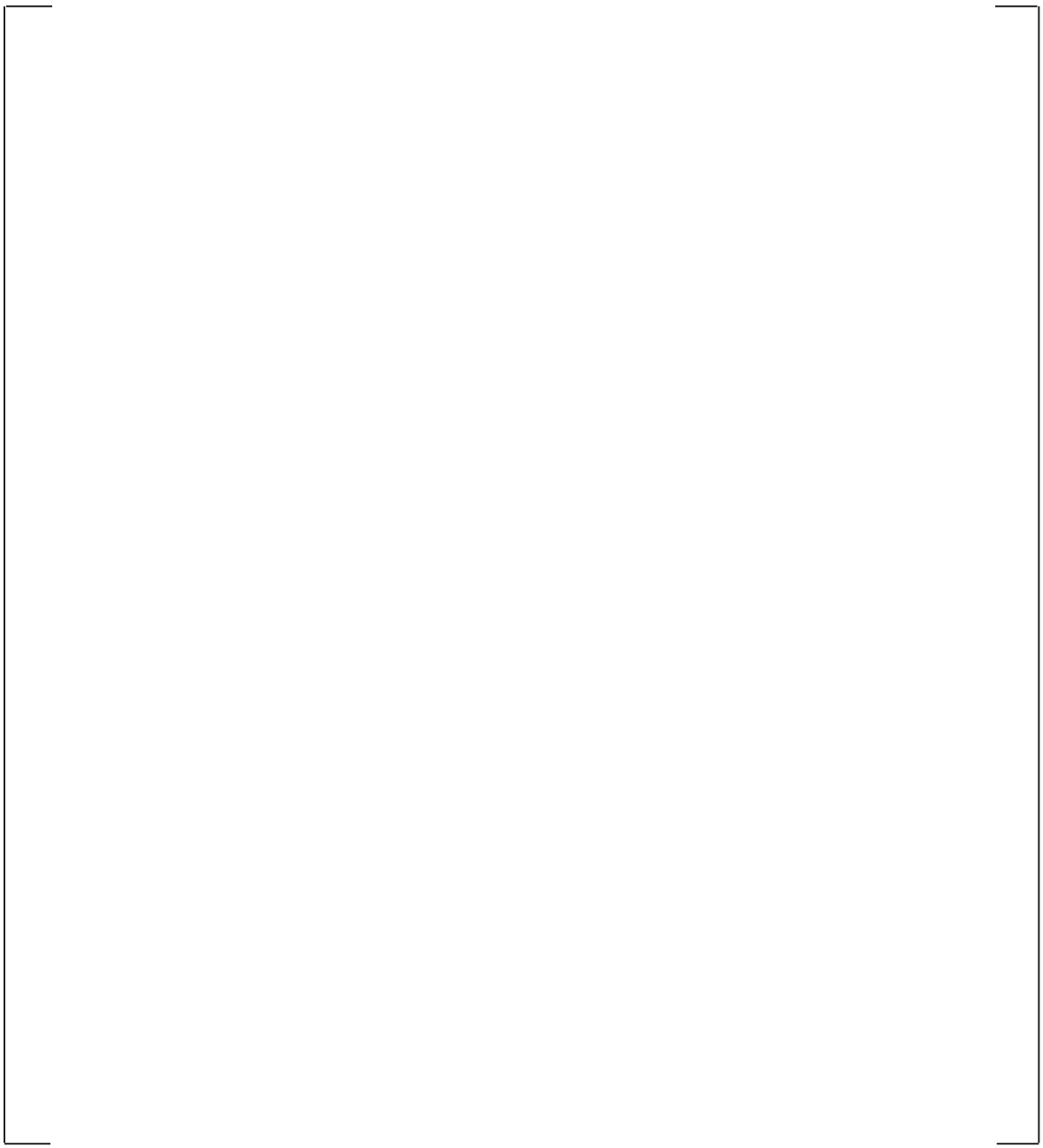

a,c

Figure 28 Equilibrium Cycle MOC Radial Peaking Factor ($F_{\Delta H}$) Distribution New versus Current NEXUS/ANC

a,c

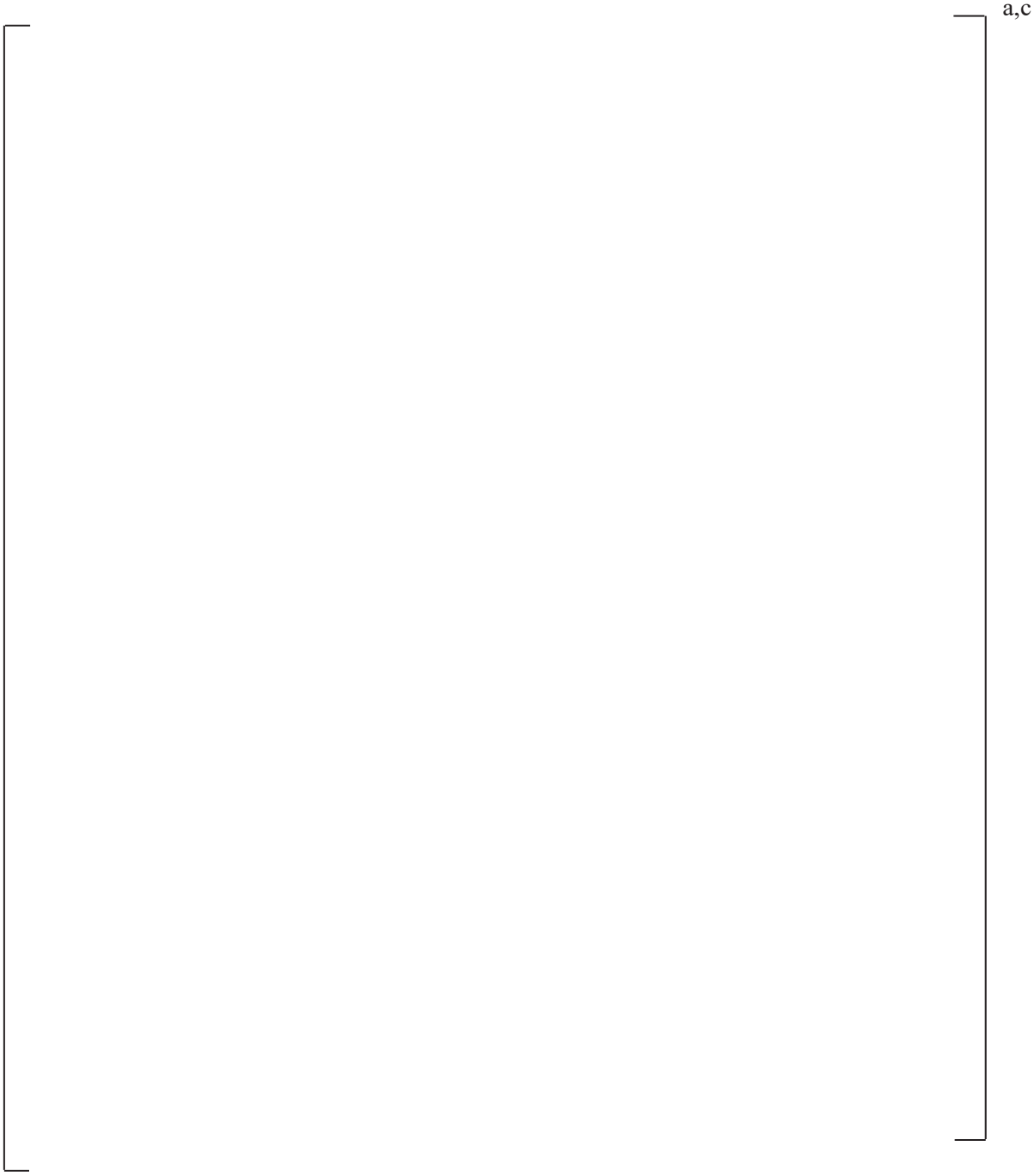

Figure 29 Equilibrium Cycle EOC Radial Peaking Factor ($F_{\Delta H}$) Distribution New and Current NEXUS/ANC

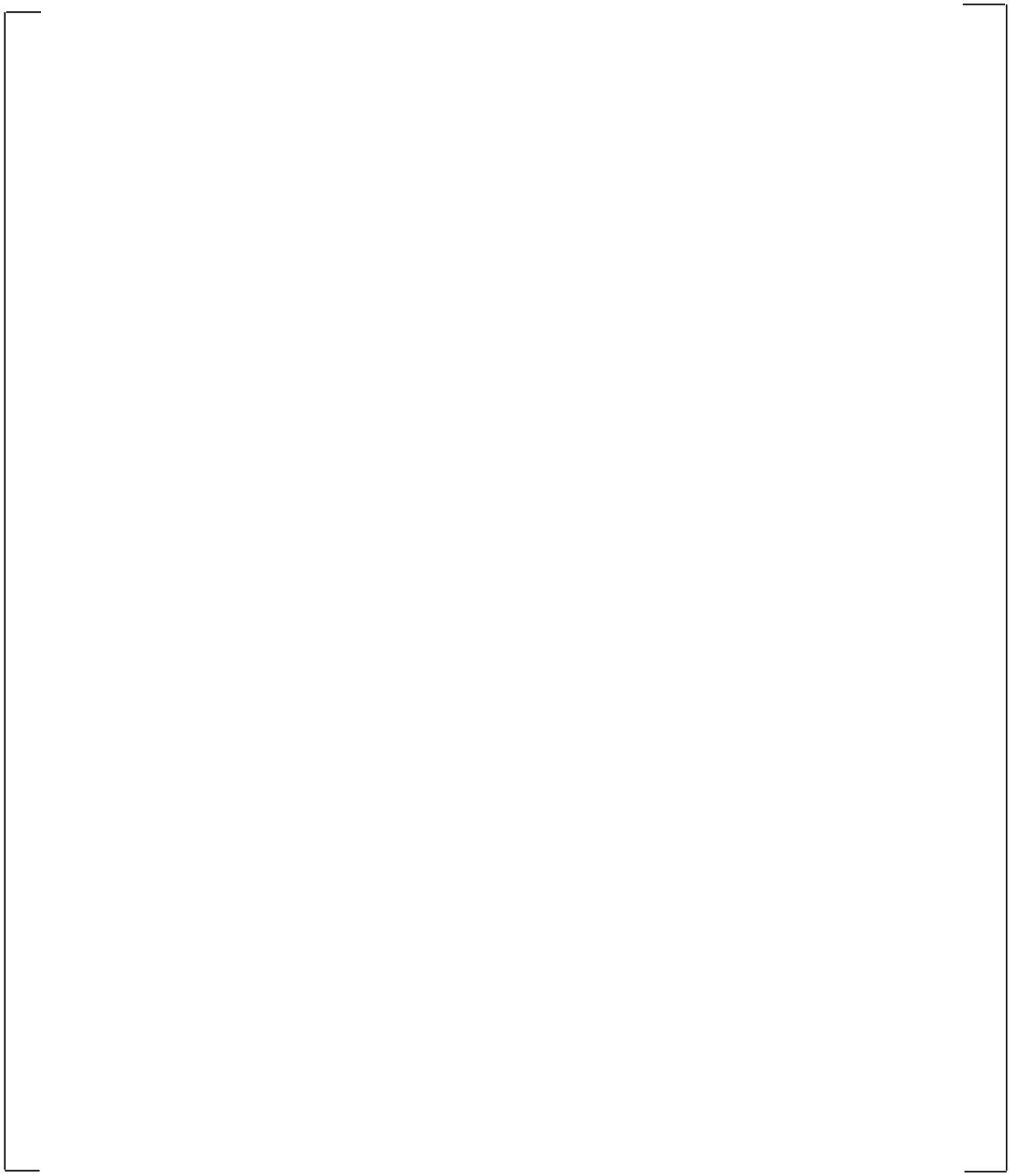

a,c

**Table 35 Hot Zero Power Control Rod Worths – Equilibrium Cycle
New versus Current NEXUS/ANC**

a,c

Table 36 Cold Reactivity Comparisons – Equilibrium Cycle

a,c

4 PROCESS FOR FUTURE CODE/METHODOLOGY MODIFICATIONS

The key indicator of the accuracy of an analytic method is the agreement of its predictions with measured data ("measured minus predicted", or "M-P", performance). Agreement between readily measurable parameters, including reactivity, rod worths, temperature coefficients and radial and axial power distribution and their calculated values, provides assurance that the reactor geometry, materials, and thermal hydraulic conditions are modeled correctly and that the analytic methods represent the core physics with sufficient accuracy. Close agreement between measured and predicted values of these key parameters validates the safety analysis for the cycle under startup or during operation.

With the anticipated future increase in computing power and speed, and increased data storage capability, Westinghouse expects to further refine the numerical methods described in this report to further improve predictive capabilities. Enhancements may, for example, include: the use of different or additional state parameters in the formulation of the nuclear cross-sections, improved thermal hydraulic modeling, improved fuel rod thermal modeling, and use of an improved multi-energy group cross-section structure.

The process that Westinghouse will use to implement future changes to the methodology is as follows. Prior to implementing such future improvements, Westinghouse will benchmark the impact of the changes on the M-P performance of ANC/NEXUS, using the criteria shown in Table 37. These criteria are based on licensed uncertainty values, or uncertainties used or assumed in the safety analysis. Meeting the criteria in Table 37 will provide sufficient validation of the methodology changes. Licensed uncertainties or previously established restrictions on the use of ANC/NEXUS will not be affected. Validations will be documented and maintained internally by Westinghouse. Changes which have been validated against the stated criteria can be used in subsequent licensing applications.

Table 37 Qualification Criteria

Parameter	M-P Agreement
Core Reactivity	500 pcm
Isothermal Temperature Coefficient	2 pcm/°F
Total control rod bank worth (where measured)	7%
Individual control rod bank worth (where measured)	Maximum of 15% or 100pcm
$F_{\Delta H}$	4%
F_Q	5%

5 SUMMARY AND CONCLUSIONS

Westinghouse has developed updated NEXUS cross-section methodologies including cross-section reformulation and re-homogenization that are designed to replace the currently licensed NEXUS methodology for PWR nuclear core design and safety analysis calculations.

In the updated NEXUS methodology presented herein, the cross-sections calculated using a standard set of lattice code calculations are **[**

][a,c] The updated methodology can more accurately simulate the fuel and core under accident scenarios, such as steamline breaks, locked rotor events, or rod ejection incidents, that can lead to a large change in core pressure or cause large local voiding conditions.

A further improvement in the updated NEXUS methodology is **[**

][a,c]

Results are presented in this report to show the accuracy of NEXUS for cross-section representation. Six different UO_2 assembly types including both Westinghouse and CE assembly types, and IFBA, WABA, and Gd_2O_3 burnable absorbers, have been calculated using the updated NEXUS method. The k-infinity results from these calculations were compared directly to PARAGON k-infinity values at the corresponding conditions. This comparison demonstrates that the NEXUS cross-sections are accurate over the range of temperatures, boron concentrations, and power levels expected to be encountered in PWR core calculations including off-nominal voided conditions, such as encountered during certain accident scenarios. Comparisons have also been made for configurations of heterogeneous adjacent assemblies (mixed core) which demonstrate that the updated NEXUS method captures the effects of the heterogeneities.

Finally NEXUS/ANC core models were developed for four actual plants (13 cycles total) and an equilibrium cycle. Results from specific cycle models were compared to actual measured values and to corresponding results from the same cycles using the currently licensed NEXUS methodology. Comparisons were made for at-power critical boron versus burnup, startup measurements, radial power distributions, rodworths, and cold reactivity calculations. For most parameters **[**

][a,c]

In conclusion, the following improvements have been incorporated in an updated NEXUS methodology:

- Provide results that are the same as or better than the currently licensed NEXUS for cross-section prediction.
- Improve the capability to calculate cross-section data under accident scenarios that result in large core pressure changes or large local voiding.
- Continue to work seamlessly with the NEXUS/ANC code system, allowing the updated NEXUS methodology to be used as a direct replacement of all existing uses of the currently licensed NEXUS methodology.

These improvements have been shown to maintain or even improve the accuracy of the NEXUS methodology. While currently licensed NEXUS remains an accurate and applicable cross-section methodology, updated NEXUS provides a broader range of capabilities and improved computational efficiency.

6 REFERENCES

1. Liu, Y. S., et al., "ANC: A Westinghouse Advanced Nodal Computer Code," WCAP-10965-P-A (Proprietary) and WCAP-10966-A (Non-Proprietary), September, 1986

2. Zhang, B., et al., "Qualification of the NEXUS Nuclear Data Methodology," WCAP-16045-P-A Addendum 1-A (Proprietary) and WCAP-16045-A (Non-Proprietary), August, 2007
3. Zhang, B., et al., "Qualification of the New Pin Power Recovery Methodology," WCAP-10965-P-A, Addendum 2-A (Proprietary) and WCAP-10966-A, Addendum 2-A (Non-Proprietary), September, 2010

4. Ouisloumen, M., et al., "Qualification of the Two-Dimensional Transport Code PARAGON," WCAP-16045-P-A (Proprietary) and WCAP-16045-NP-A (Non-Proprietary), August, 2004

5. Zhang, B., et al, "Application of Westinghouse NEXUS/ANC9 Cross-Section Model for PWR Accident Analysis," PHYSOR2014, The Role of Reactor Physics Toward a Sustainable Future, Kyoto, Japan, September 28 ~ October 3, 2014